AD-A093 971 ROYAL AIRCRAFT ESTABLISHMENT FARNBOROUGH (ENGLAND) F/G 20/4
LEADING-EDGE SEPARATION FROM A SLENDER ROLLING WING-BODY COMBIN--ETC(U)
MAR 80 I JONES
UNCLASSIFIED RAE-TR-80039 DRIC-BR-74711 NL

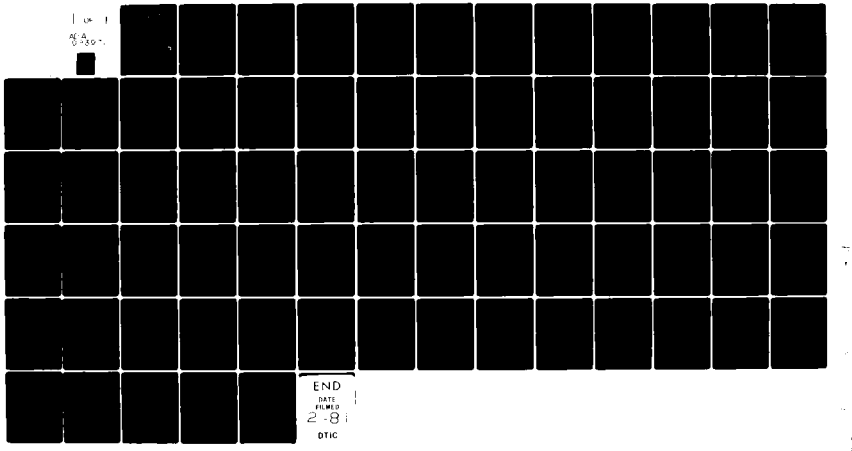

END
DATE FILMED
2-81
DTIC

UNLIMITED

(14) RAE-TR-80039

(18) DRIC (19) BR-74711

LEVEL II

4

B.S.

ROYAL AIRCRAFT ESTABLISHMENT

*

(9) Technical Report 80039

(11) Mar 80 (12) 73

UNLIMITED

(6) LEADING-EDGE SEPARATION FROM A SLENDER ROLLING WING-BODY COMBINATION.

by

(10) I.P. Jones

*

Procurement Executive, Ministry of Defence

Farnborough, Hants

UDC 533.691.1 : 533.6.048.3 : 533.695.12 : 533.6.013.153

4

ROYAL AIRCRAFT ESTABLISHMENT

Technical Report 80039

Received for printing 13 March 1980

LEADING-EDGE SEPARATION FROM A SLENDER ROLLING WING-BODY COMBINATION

by

I. P. Jones*

SUMMARY

A vortex-sheet model of the leading-edge separation is used to study the flow about a slender wing-body combination in steady rolling motion at zero incidence. The equations which model the flow are derived and the numerical method to solve these equations is described. The results presented concentrate on those values of the parameters for which comparison may be made with the experimental results of Harvey for a rolling delta wing. Results obtained using simplified flow models are also described.

Departmental Reference: Aero 3476

* Computer Science and Systems Division, AERE Harwell. The bulk of this work was carried out at the School of Mathematics and Physics, University of East Anglia, under a research agreement between the University and the Ministry of Defence, monitored by Aerodynamics Department, RAE.

LIST OF CONTENTS

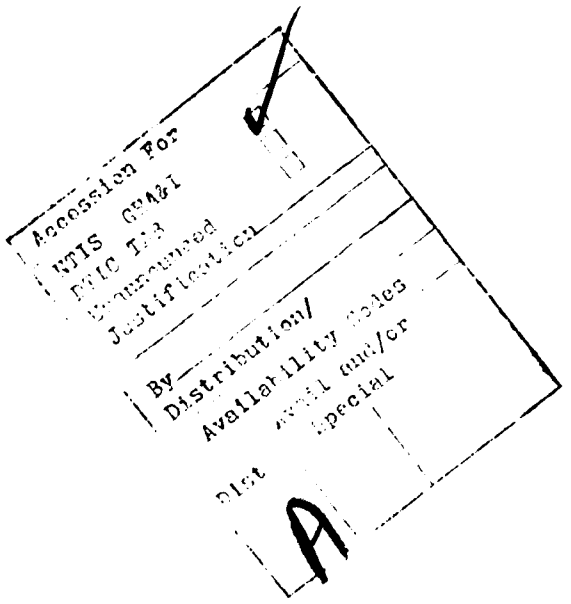

1 INTRODUCTION

In this Report we consider a wing-body combination, consisting of a slender wing mounted symmetrically on a circular cylinder, and rolling steadily about the axis of the cylinder, which is aligned with a uniform stream. The flow is assumed to separate at the leading edges of the wing.

When a plane slender wing is at incidence to a uniform stream, the boundary layers on its upper and lower surfaces leave the leading edges to coalesce into free shear layers which spiral into vortex cores lying above the upper surface of the wing. The flow is observed to be steady and stable, and it is possible to exploit the characteristics of the leading-edge vortices, particularly to enhance the lift of the wing at low speeds.

If the wing at incidence acquires a rolling motion, fast enough to produce a helix angle at the wing tip as large as the angle of incidence, the simplicity of this flow pattern is destroyed. At some station along the ascending leading edge the shear layer will cease to feed the upper surface vortex found upstream and will instead roll up into a second vortex below the wing. Multiple vortices will also form from the leading edges of a wing oscillating in roll at zero incidence. The basic simplicity of the wing at incidence is preserved in two cases: the wing at incidence and with small disturbances in roll, and the wing at zero incidence in steady roll. In the former the pair of vortices still lie above the upper surface of the wing: in the latter they lie on opposite surfaces of the wing, below the ascending panel and above the descending panel. The latter problem was chosen for the present investigation because the nonlinear effects were expected to be larger.

The conical laterally symmetric problem, associated with a slender delta wing at incidence, has attracted considerable attention because it is the simplest problem which exhibits the characteristic features of this important type of real flow. In the first attempts to model such a flow[1,2] the vortex core and shear layer were replaced by an isolated potential vortex but the resulting solutions, when compared with experimental results, were unsatisfactory. To overcome the limitations of the isolated vortex model, Mangler and Smith[3] included some of the effects of the shear layer by incorporating into their model a finite vortex sheet of simple form which extended from the leading edge of the wing towards the core of the vortex. The agreement with the measured lift was better than that achieved with the earlier models but the vortex position was still not predicted satisfactorily.

With the advent of high speed computers Smith[4] obtained the first satisfactory solutions to the original problem. The model he used was similar to that of Mangler and Smith, except that the shape and strength of the vortex sheet were not constrained to any predefined forms. His method of solution reduced the equations which express the boundary conditions, and so determine the position and strengths of the vortex core and sheet, to a set of nonlinear algebraic equations which was solved using a nested iteration scheme. The numerical scheme owed its origins to some extent to physical insight and associated certain variables with certain equations. This method gave, at best, linear convergence. For low values of the incidence this scheme fails to converge and Barsby[5], using a more accurate representation of the sheet, together with an improved iterative procedure, was able to extend the range of solutions to include extremely small incidences.

The assumptions made by Smith[4] in his study of the symmetric conical flow, which are described in more detail in his paper, are adopted in this Report and are as follows.

(1) The flow is effectively inviscid. This assumption is substantiated by experimental observations which indicate that viscosity is important only in the thin boundary layers on the surface of the wing, a region of secondary separation underneath the vortex core, in the shear layers and in a small region of the vortex core. The experiments confirm that most of the large-scale features of the flow are independent of the Reynolds number. The secondary separation which is induced by an adverse pressure gradient caused by the primary vortex is ignored in this model.

(2) The vorticity in the fluid is condensed onto vortex sheets which emanate from the leading edges. Each sheet is infinite in length and rolls up into a tight spiral core. This infinite sheet is replaced by a finite outer part springing from the leading edge and an isolated potential vortex. The circulation on the spiral core is condensed onto the isolated vortex leaving behind a trace. Across this trace there is a discontinuity of pressure and fluid speed that is independent of its shape. This trace is represented by a cut which joins the isolated vortex to the free end of the finite vortex sheet. This approximation appears to be adequate to describe the flow outside the core region.

(3) The slender-body theory of Munk, Jones and Ward[20] is used. Thus the velocity potential satisfies Laplace's equation in planes perpendicular to the main flow, the cross-flow plane. This theory neglects the influence of the trailing edge which is important for an upstream distance of the order of the

wing span at low speeds. The results obtained are independent of Mach number but deteriorate as the reduced aspect ratio $(A\sqrt{M^2 - 1})$ increases for $M > 1$.

The effect of these assumptions is to reduce the problem to that of finding a velocity potential which satisfies the two-dimensional form of Laplace's equation subject to zero normal velocity on the wing, an appropriate condition at infinity due to the incident flow and certain conditions on the vortex sheet, the isolated vortex and cut, and at the leading edge.

The boundary conditions on the vortex sheet are that the vortex sheet is a stream surface of the three-dimensional flow, the stream-surface condition; and that the pressure is continuous across the vortex sheet, the pressure condition. It is impossible, however, to satisfy a pressure condition on the isolated vortex and cut and the best that can be achieved[4] is to make both transverse components of the overall force acting on this system zero. Finally a Kutta condition, that the velocity is finite at the leading edge, is applied.

Using this vortex sheet model several authors[6-11] have studied a number of conical flow configurations.

For configurations with lateral symmetry, making the overall force on each vortex and cut vanish automatically ensures that there is no net rolling moment carried by the fluid. For yawed wings it is possible[9,10] to choose the extent of the vortex sheets from the two leading edges so as to minimise the net rolling moment in the fluid. In the present problem, on the other hand, central symmetry implies that the rolling moments which remain on each vortex-and-cut system are equal and cannot combine to give zero overall moment. However the residual rolling moment in the fluid is small compared to the rolling moment on the wing and is ignored in the present treatment.

More fundamentally the problem of the rolling wing is not conical, even for a delta wing in the slender-body approximation, since the disturbance produced by elements of the wing depends on their distance from the axis of roll and this increases as the distance from the apex increases along each conical ray. This means that the solution in each cross-flow plane depends in a more complicated manner upon the upstream conditions. Early attempts[12,13] to study non-conical flows used simplified flow models based on that of Brown and Michael[2]. The boundary conditions on a non-conical vortex-sheet embedded in a steady potential flow have been derived by Smith[14]. Using these boundary conditions Smith[15] has obtained similarity solutions for two classes of wing for which conical flow emerges as a special case. More recently Clark[16] and Jones[17] have developed

numerical marching schemes for dealing with slender wings of arbitrary planform. Other models have been developed to attack non-conical flow problems, for example by Sacks *et al*[18], with varying degrees of success. A reasonably accurate method for predicting forces and moments on wings with edge separation is based on the leading-edge suction analogy of Polhamus[19]. This analogy states that the non-linear component of the force acting normal to the wing in separated flow is equal to the suction force acting in the plane of the wing due to the singular behaviour of the attached flow at the sharp edge. Despite the success of the analogy it has not been possible so far to provide a wholly rational basis for it.

In this Report we are primarily concerned with the separated flow over a wing-body combination at zero incidence rolling steadily about its axis with angular velocity Ω in a free stream of velocity U. The wing-body combination consists of a slender delta wing of semi-apex-angle γ mounted symmetrically on a circular cylinder of radius r. The span of the configuration is $2s$. This configuration is sketched in Fig 1. The mathematical model and numerical method are, however, applicable to a slender wing of general planform symmetrically mounted on a circular cylinder. As explained later, solutions can be obtained which approximate those for isolated wings.

Relative to any set of non-rotating axes, the flow considered is time-dependent. However, by introducing axes which rotate with the configuration, the problem is reduced to an equivalent problem in steady flow with a pre-determined distribution of rotation in the fluid.

In section 2, the attached flow solution to this problem is obtained, using the conformal mapping of the region of the cross-flow plane occupied by the fluid on to the region of the transformed plane exterior to a circle. The separated flow is then represented by introducing vortex sheets and isolated vortices into the attached flow field, together with their images in the circle in the transformed plane. In this way, the boundary conditions on the wing and body, satisfied by the attached flow, are preserved. Details of the construction of the separated flow model are given in section 4.

The boundary conditions which must be satisfied on the non-conical vortex sheet in the rolling motion are derived in section 3, following the derivation of Ref 14. The zero force condition, expressing the vanishing of the total force on the isolated vortex and cut which represents the core, and the Kutta condition at the leading edge are formulated in section 4. These conditions take the form of ordinary differential equations which are sufficient to define the rates of change, in the streamwise direction, of the position and strength of the isolated

vortex and of the shape and strength of the vortex sheets, in terms of the velocity field in the cross-flow plane.

Near the apex of the exposed wing, point A in Fig 1, the semi-span of the exposed wing is small in comparison with the body radius, so that the body side appears as an infinite reflection plane. Moreover, the relative velocity between the wing and the undisturbed fluid is approximately uniform over a small region, so the flow near A resembles that of a delta wing at an angle of incidence equal to $r\Omega/U$. Hence the flow near A may be obtained from a known conical solution. This provides the initial conditions for the set of ordinary differential equations described above, so that the solution is now, in principle, determined.

The numerical solution of these equations is described in section 5. The process falls into a number of distinct stages. The representation of the vortex sheet in the cross-flow plane is discretised, so that the unknowns become a finite set of coordinates and strengths, and the boundary conditions become a finite set of ordinary differential equations. The streamwise derivatives which occur in these equations are represented by central differences in an implicit formulation. This formulation requires the solution of a set of simultaneous nonlinear equations for the values of the coordinates and strengths of the sheet and isolated vortex in each cross-flow plane, each set of equations depending on the solution already found for cross-flow planes further upstream. These simultaneous nonlinear equations are solved by a multi-dimensional form of the Newton-Raphson method. Because the initial conditions obtained from the conical solution for the wing at incidence are not exactly appropriate to the rolling problem, instabilities can arise in the first few steps of the downstream integration. These are overcome by an averaging process.

The only detailed experimental results available for comparison are those of Harvey[21], for an isolated delta wing of semi-apex angle 10^{o}. He obtained measurements in three cross-flow planes at three different rates of roll, in an essentially incompressible flow. The present calculations have been directed towards obtaining results for these nine cross-flows. The results obtained are discussed in section 6 in relation to Harvey's observations. As described above, the presence of the body is an essential feature of the calculation method. In principle, the body can be made as small as we please, relative to the overall wing span at the station of interest. In practice this means that the conical starting solution corresponds to a very weak separation, for which difficulties arise[5] in obtaining the appropriate solution. However it emerges that solutions virtually independent of the body size can be found for bodies small compared with

the local span. To provide an indication of the influence of body size on the separated flow, the isolated vortex model of Brown and Michael[2] was also formulated for the wing-body combination and results calculated for comparison with the results of Hanin and Mishne[22] for the wing alone. Finally, the leading-edge suction analogy of Polhamus was applied, within the context of slender-body theory, to the wing-body combination. The results are discussed in section 6.

2 THE COMPLEX POTENTIAL FOR ATTACHED FLOW

Within the framework of slender-body theory we are concerned with solutions of Laplace's equation in the cross-flow plane. Since this equation is linear and the boundary conditions on the wing and body and at infinity are also linear, the velocity field of the separated flow may be constructed by superposing a representation of the leading-edge vortices on the attached flow solution. In this section therefore we consider the attached flow problem for the rolling wing-body combination described in the last section and illustrated in Fig 1.

We define a right-handed set of Cartesian axes (x, y, z) fixed in space with the origin O on the axis of the body in the cross-flow plane through the apex of the exposed wing. The x-axis is along the axis of the body in the downstream direction and, at the instant of time that we are considering, $t = 0$ say, the y-axis is in the direction of the starboard wing, as shown in Fig 1. This frame of reference, since it is fixed in space, we shall call the 'inertial frame'. We also find it convenient to work with another frame of reference, the 'rotational frame', with a set of Cartesian axes fixed in the body such that at the same instant of time, $t = 0$, these two sets of axes are coincident. In this rotational frame the flow is steady but it is not a potential flow. In the inertial frame, however, the flow is an unsteady potential flow and in the remainder of this section we shall work entirely within this inertial frame at the instant $t = 0$.

We make use of slender-body theory and since, in the absence of separation, no vorticity is being convected downstream the velocity field in each cross-flow plane is entirely determined within that plane. Hence, for the flow in each cross-flow plane, we may define a complex potential

$$W_A(Z) = \phi + i\psi$$

where $Z = y + iz$ with ϕ the velocity potential and ψ the stream function. The effect of the free stream is not included in W_A.

The boundary condition which must be satisfied on the wing-body combination is that the normal velocity relative to the wing-body is zero. Hence, on the wing

$$\frac{\partial \Phi}{\partial z} = \Omega y \qquad \text{for } z = 0 \text{ and } r \leq |y| \leq s \tag{1}$$

where Ω is the angular velocity about the positive x-axis. Note that Fig 1 is drawn for a negative value of Ω. On the body

$$\frac{\partial \Phi}{\partial n} = 0 \qquad \text{for } \sqrt{y^2 + z^2} = r \tag{2}$$

where n is the unit vector normal to the body. At infinity the fluid is at rest and so we have

$$\frac{dW}{dZ} \to 0 \qquad \text{as } Z \to \infty \ . \tag{3}$$

Using various methods, several authors have considered problems of rolling wing-body and cruciform-tail-body combinations, for example, Lomax and Heaslett[23], Adams and Dugan[24] and Bobbit and Malvestuto[25]. The method used here is based on that presented by Adams and Dugan for a rolling cruciform-tail-body combination and introduces a distribution of doublets on the surface of the wing to satisfy the boundary conditions (1) and (2).

First we transform the region of the cross-flow plane outside the cross section of the wing-body combination onto the exterior of the unit circle in the transformed plane. By a Joukowski transformation the cylindrical body can be transformed into a slit lying on the real axis. The wing itself, since it lies on the real axis in the physical plane, is merely transformed into an extension of the same slit along the real axis under this transformation. Thus the transformation

$$Z^* = \frac{s}{s^2 + r^2}\,(Z + r^2/Z)$$

is such that the wing-body combination is represented in the Z^* plane by the slit

$$-1 < Z^* < 1 \ .$$

This slit is mapped, again with the aid of a Joukowski transformation, into the unit circle $|\zeta| = 1$. The complete transformation of the wing-body combination into the unit circle is then given by

$$\frac{1}{2}\left(\zeta + \frac{1}{\zeta}\right) = Z^* = \frac{s}{s^2 + r^2}\left(Z + \frac{r^2}{Z}\right) \tag{4}$$

where ζ is the point in the final transformed plane corresponding to the point Z in the physical plane.

In this transformed plane we see from (4) that the points ζ on the arc of the circle representing the upper surface of the starboard wing, $r < y < s$, are given by

$$\left.\begin{aligned} \zeta &= e^{i\theta} \qquad\qquad 0 < \theta < \theta_1 \\ \text{where} \qquad \theta_1 &= \cos^{-1}\frac{2rs}{s^2 + r^2} \end{aligned}\right\} . \tag{5}$$

Similarly points on the lower surface of the starboard wing are given by

$$\zeta = e^{-i\theta}$$

and on the upper and lower surfaces of the port wing by

$$\zeta = -e^{-i\theta} \quad \text{and} \quad \zeta = -e^{+i\theta}$$

respectively, for $0 < \theta < \theta_1$ as shown in Fig 2a.

Let us now consider a source of strength m at a point $\zeta = e^{i\theta}$, $0 < \theta < \pi$, on the unit circle and a sink of strength m at the point $\zeta = e^{-i\theta}$ as shown in Fig 2b. The complex potential for this source-sink configuration at some point ζ_0 in the transformed plane is

$$W_A(\zeta_0) = \frac{m}{2\pi}\log\left\{\frac{\zeta_0 - e^{i\theta}}{\zeta_0 - e^{-i\theta}}\right\} . \tag{6}$$

From this we can easily recover the classical result that the stream function is piece-wise constant on the unit circle, so that the source-sink combination induces no normal velocity on the contour except at the locations of the source and sink. This source-sink pair corresponds to a doublet of strength m in the physical plane where we again have zero normal velocity everywhere on the wing-body except at the location of the doublet itself. Furthermore, because we effectively have a source on the upper surface of the wing and a sink on the lower surface the velocity of the fluid normal to the wing-body at the location of the doublet is in the same direction on both sides of the wing, as is required from (1).

We now consider a distribution of doublets along the wing. This automatically satisfies the condition of zero normal velocity on the body (2) as we have seen, and the boundary condition (3) at infinity. From the continuity of mass flow across the surface we require

$$dm = 2 \frac{\partial \Phi}{\partial z} dy \tag{7}$$

where dm represents the strength of the doublet on the segment dy of the wing in the physical plane and $\partial\Phi/\partial z$ is given by (1). From this distribution of doublets on the wing we have, at the point ζ_0 in the transformed plane,

$$W_A(\zeta_0) = \frac{1}{2\pi} \int_{y=-s}^{y=-r} dm \log \left\{ \frac{\zeta_0 - \zeta(y)}{\zeta_0 - \bar{\zeta}(y)} \right\} + \frac{1}{2\pi} \int_{y=r}^{s} dm \log \left\{ \frac{\zeta_0 - \zeta(y)}{\zeta_0 - \bar{\zeta}(y)} \right\} \tag{8}$$

where $\zeta(y)$ is the point in the transformed plane corresponding to the point y on the wing in the physical plane and the bar denotes the complex conjugate. Introducing (1) into (7) and then substituting the result into (8) we obtain for the attached flow potential

$$W_A(\zeta_0) = \int_{y=r}^{y=s} \frac{\Omega y}{\pi} \log \left(\frac{\zeta_0^2 - \zeta^2(y)}{\zeta_0^2 - \bar{\zeta}^2(y)} \right) dy \tag{9}$$

using the result $\zeta(-y) = -\bar{\zeta}(y)$.

If we now write $\zeta = e^{i\theta}$ and integrate (9) by parts we get

$$W_A = \left[\frac{\Omega y^2}{2\pi} \log \frac{\zeta_0^2 - \zeta^2}{\zeta_0^2 - \bar{\zeta}^2}\right]_{y=r}^{y=s} + \int_0^{\theta_1} \frac{\Omega y^2}{2\pi} \left\{ \frac{-2i\zeta e^{i\theta}}{\zeta_0^2 - \zeta^2} \frac{-2i\bar{\zeta} e^{-i\theta}}{\zeta_0^2 - \bar{\zeta}^2} \right\} d\theta \qquad (10)$$

since, from (5), $\theta = 0$ when $y = s$ and $\theta = \theta_1$ when $y = r$.

From (4) and (5), since $Z = y$ on the wing, we have

$$y^2 - 2yr \frac{\cos\theta}{\cos\theta_1} + r^2 = 0 \quad . \qquad (11)$$

The integrals in (10) may now, with the aid of (11), be evaluated, using standard techniques. The details of the integration may be found in Jones[26]. The complete expression for W_A is given by

$$\left.\begin{aligned} W_A = &- \frac{\Omega r^2}{2\pi} \log\left(\frac{\zeta^2 - e^{2i\theta_1}}{\zeta^2 - e^{-2i\theta_1}}\right) + \frac{i\Omega r^2(\zeta^4 - 1)\theta_1}{2\pi\zeta^2 \cos^2\theta_1} \\ &- \frac{1}{2} \frac{\Omega r^2}{\pi \cos^2\theta_1} \left(\tfrac{1}{2}\chi + \sin^2\theta_1\right) \log\left(\frac{(\zeta^2 - 1) + i \tan\theta_1(\zeta^2 + 1)}{(\zeta^2 - 1) - i \tan\theta_1(\zeta^2 + 1)}\right) \\ &+ \frac{i\Omega(\zeta^4 - 1)r^2}{4\zeta^2 \cos^2\theta_1} - \frac{i\Omega r^2}{4 \cos^2\theta_1} \frac{\zeta^2 + 1}{\zeta^2} \sqrt{\zeta^4 - 2\cos 2\theta_1 \zeta^2 + 1} \end{aligned}\right\} \qquad (12)$$

where $\chi = \zeta^2 + 1/\zeta^2$ and the suffix zero has been dropped from ζ_0.

By differentiating this expression for constant x, the corresponding complex velocity in the transformed plane may easily be found as

$$\frac{dW_A}{d\zeta} = \left.\begin{aligned} &- \frac{2i\Omega r^2 \sin 2\theta_1}{\pi\zeta\left(\zeta^2 + \frac{1}{\zeta^2} - 2\cos 2\theta_1\right)} + \frac{i\Omega r^2\theta_1}{\zeta\pi\cos^2\theta_1}\left\{\zeta^2 + \frac{1}{\zeta^2}\right\} \\ &- \frac{1}{2}\frac{\Omega r^2}{\pi\cos^2\theta_1}\frac{1}{\zeta}\left(\zeta^2 - \frac{1}{\zeta^2}\right)\log\left\{\frac{(\zeta^2 - 1) + i\tan\theta_1(\zeta^2 + 1)}{(\zeta^2 - 1) - i\tan\theta_1(\zeta^2 + 1)}\right\} \\ &+ \frac{4i\Omega r^2\tan\theta_1}{\pi\cos^2\theta_1}\left\{\frac{1}{2}\left(\zeta^2 + \frac{1}{\zeta^2}\right) + \sin^2\theta_1\right\}\frac{\zeta}{\left((\zeta^2 - 1)^2 + \tan^2\theta_1(\zeta^2 + 1)^2\right)} \\ &+ \frac{i\Omega r^2}{2\cos^2\theta_1\zeta}\left(\zeta^2 + \frac{1}{\zeta^2}\right) + \frac{i\Omega r^2}{2\cos^2\theta_1\zeta^3}\sqrt{\zeta^4 - 2\cos 2\theta_1\zeta^2 + 1} \\ &- \frac{i\Omega r^2}{2\cos^2\theta_1}\frac{(\zeta^2 + 1)}{\zeta}\frac{\left(\zeta^2 - \cos 2\theta_1\right)}{\sqrt{\zeta^4 - 2\cos 2\theta_1\zeta^2 + 1}} \quad . \end{aligned}\right\} \qquad \ldots\ldots(13)$$

From this complicated expression (13) it may be verified directly that we have the required complex velocity in the transformed plane which satisfies conditions (1) on the wing, (2) on the body and (3) at infinity. Care must, however, be taken when evaluating the complex logarithms and square roots in (13) to accommodate the changes from one branch to another which may be encountered on that part of the boundary in the ζ-plane which corresponds to the wing. This is because for a point ζ on the boundary the integrand in (9) becomes singular. Hence to calculate $\partial W_A/\partial\zeta$ at $\zeta = e^{i\theta}$, say, from (13) we must evaluate

$$\lim_{\epsilon\to 0}\frac{dW_A}{d\zeta}\left((1 + \epsilon)e^{i\theta}\right) \quad ,$$

where ϵ is real and positive, to ensure that the correct values are obtained.

Knowing the attached flow potential and the corresponding complex velocity through (12) and (13) we are now, as mentioned in section 1, in a position to construct the complex velocity in the presence of leading-edge separation. This is carried out in section 4. First, however, in section 3 we derive the boundary conditions to be satisfied on a steadily rolling vortex sheet.

3 THE BOUNDARY CONDITIONS ON A STEADILY ROLLING VORTEX SHEET

In this section we discuss in detail the boundary conditions to be satisfied on a vortex sheet which is rolling steadily about an axis parallel to an oncoming stream. As we have discussed in section 1, the conditions that must be satisfied are continuity of pressure across the sheet, the pressure condition, and the condition that the vortex sheet is a stream surface of the three-dimensional flow, the stream-surface condition.

In a rotating frame of reference the motion is not a potential flow. However if we consider a set of axes (x, y, z) in the inertial frame defined in the previous section, that is fixed in space, with the wing rotating about the x-axis with constant angular velocity $\underline{\Omega} = (\Omega, 0, 0)$, then relative to these axes the flow is an unsteady potential flow. Hence, from Bernoulli's theorem we have

$$\frac{\partial \Phi}{\partial t} + \tfrac{1}{2}\underline{u} \cdot \underline{u} + \frac{p}{\rho} = c(t) \tag{14}$$

where $\underline{u} = \nabla\Phi$. Thus, from continuity of pressure across the sheet we have

$$\Delta\left(\frac{\partial \Phi}{\partial t} + \tfrac{1}{2}\underline{u} \cdot \underline{u}\right) = 0 \tag{15}$$

where Δ is the difference operator across the seeet, 'inside minus outside'.

In order to relate $\partial\Phi/\partial t$ to the velocity field, we first introduce Cartesian axes in the rotating frame, fixed to the wing, and therefore rotating about the x-axis of the inertial frame with constant angular velocity Ω . If the new y' and z' axes coincide with the inertial y and x axes at time $t = 0$ the coordinates are related by:

$$\left.\begin{aligned} y' &= y\cos\Omega t + z\sin\Omega t \\ z' &= z\cos\Omega t - y\sin\Omega t \\ y &= y'\cos\Omega t - z'\sin\Omega t \\ z &= y'\sin\Omega t + z'\cos\Omega t \end{aligned}\right\} \tag{16}$$

The velocity vector $\underline{q}$, relative to the new axes is given by

$$\underline{u} = \nabla\Phi = \underline{q} + \underline{\Omega} \wedge \underline{r} \tag{17}$$

(Greenspan)[27], where $\underline{r}$ is the radius vector from the origin and the gradient operator is relative to the inertial frame. Since the flow is steady in the new axes, we write

$$\Phi(x, y, z, t) = F(x, y', z')$$

so that

$$\frac{\partial \Phi}{\partial t} = \frac{\partial F}{\partial y'}\frac{\partial y'}{\partial t} + \frac{\partial F}{\partial z'}\frac{\partial z'}{\partial t}$$

$$= \Omega\left(z' \frac{\partial F}{\partial y'} - y' \frac{\partial F}{\partial z'}\right) \qquad (18)$$

by (16).

Similarly we find

$$\frac{\partial F}{\partial y'} = \frac{\partial \Phi}{\partial y}\frac{\partial y}{\partial y'} + \frac{\partial \Phi}{\partial z}\frac{\partial z}{\partial y'}$$

$$= \cos \Omega t \frac{\partial \Phi}{\partial y} + \sin \Omega t \frac{\partial \Phi}{\partial z}$$

and

$$\frac{\partial F}{\partial z'} = -\sin \Omega t \frac{\partial \Phi}{\partial y} + \cos \Omega t \frac{\partial \Phi}{\partial z} \quad .$$

Hence, by (18),

$$\frac{\partial \Phi}{\partial t} = \Omega\left(z \frac{\partial \Phi}{\partial y} - y \frac{\partial \Phi}{\partial z}\right) \quad . \qquad (19)$$

Since $\underline{\Omega} = (\Omega, 0, 0)$, equation (17) can be written as

$$\underline{q} = \underline{u} - (0, -\Omega z, \Omega y), \qquad \text{with } \underline{u} = \nabla\Phi \ .$$

Now, forming the scalar product and taking the difference across the sheet at the same point (y, z), we have

$$\Delta(\underline{q} \cdot \underline{q}) = \Delta\left(\underline{u} \cdot \underline{u} + 2\Omega z \frac{\partial \Phi}{\partial y} - 2\Omega y \frac{\partial \Phi}{\partial z}\right)$$

$$= \Delta\left(\underline{u} \cdot \underline{u} + 2 \frac{\partial \Phi}{\partial t}\right) \qquad \text{by (19)}$$

$$= 0 \qquad \text{by (15)} \ .$$

We may therefore replace the pressure condition (15) by

$$\Delta(\underline{q} \cdot \underline{q}) = 0 \quad . \tag{20}$$

In other words the jump in the magnitude of the velocity in the rotational frame, in which we find it convenient to work, is zero.

The second boundary condition, as mentioned earlier, is that the vortex sheet is a stream surface. Thus

$$\underline{q} \cdot \underline{n} = 0 \tag{21}$$

where $\underline{n}$ is the unit vector normal to the surface.

These conditions (20) and (21) are now similar to those used by Smith[14] in his derivation of the boundary condition for steady potential flow, except that the actual velocity $\underline{u}$ which appears in his conditions is replaced by the relative velocity $\underline{q}$ in the rotating frame. For this reason the following analysis follows closely that of Smith although some of the detail is omitted. Our aim is to express the boundary conditions (20) and (21) in forms which are suitable for a numerical calculation. The first step is to express them in terms of quantities defined on the section of the vortex sheet by a plane normal to the free stream.

We define a coordinate system (ξ, η, ψ) with ξ as a coordinate measured in the direction of the uniform stream, and with η and ψ as coordinates in the cross-flow plane normal to the uniform stream. The vortex sheet Σ, being a stream surface, cannot lie entirely in a plane ξ = constant and the coordinate system is chosen so that Σ does not lie in a surface η = constant. This configuration is shown in Fig 3. We define $\underline{a}$ and $\underline{b}$ as unit vectors in the tangent plane to the sheet with $\underline{a}$ in the direction of constant η and increasing ξ, and $\underline{b}$ in the direction of constant ξ and increasing η. At the point P which we are considering $\underline{a} \wedge \underline{b}$ is normal to the sheet and hence the stream surface condition (21) $\underline{q} \cdot \underline{n} = 0$, may be written as

$$[\underline{a} \wedge \underline{b}] \cdot \underline{q}_1 = [\underline{a} \wedge \underline{b}] \cdot \underline{q}_2 = 0 \tag{22}$$

where $\underline{q}$ is the velocity vector relative to the rotating frame and the subscript 1 refers to quantities on the inside of the sheet with reference to the direction of the vector $\underline{a} \wedge \underline{b}$, and the subscript 2 to quantities on the outside of the sheet.

We can form a set of orthogonal axes with unit vectors $\underline{i}$, $\underline{b}$ and $\underline{i} \wedge \underline{b}$, where $\underline{i}$ is the unit vector in the streamwise direction and consequently $\underline{i} \wedge \underline{b}$

is directed towards the inside of Σ along the normal to the section of Σ by the plane ξ = constant . If, therefore, we write $\underline{q}$ as

$$\underline{q} = (U + q_\xi)\underline{i} + q_t\underline{b} + q_n\underline{i} \wedge \underline{b} \tag{23}$$

and take the scalar product of this equation with $\underline{a} \wedge \underline{b}$, we obtain from (22)

$$(\underline{a} \wedge \underline{b}) \cdot \underline{i}(U + q_\xi) + (\underline{a} \cdot \underline{i})q_n = 0 \tag{24}$$

since $(\underline{a} \wedge \underline{b}) \cdot \underline{b} = 0$ and $(\underline{a} \wedge \underline{b}) \cdot (\underline{i} \wedge \underline{b}) = \underline{a} \cdot \underline{i}$. For small disturbances $q_\xi \ll U$ we obtain for the stream surface condition (24):

$$\frac{q_n}{U} = -\frac{(\underline{a} \wedge \underline{b}) \cdot \underline{i}}{\underline{a} \cdot \underline{i}} \tag{25}$$

a condition which applies on both sides of the vortex sheet.

The pressure condition (20) may now, from (23), be written as

$$\Delta\left\{(U + q_\xi)^2 + q_t^2 + q_n^2\right\} = 0 \quad .$$

We have then, again assuming $q_\xi \ll U$,

$$U\Delta q_\xi + q_{tm}\Delta q_t = 0 \tag{26}$$

where q_{tm} is the mean velocity component tangential to the section of the sheet by the cross-flow plane:

$$q_{tm} = \tfrac{1}{2}(q_{t1} + q_{t2})$$

and the continuity of q_n across the sheet, expressed by (25) has been used.

Since the component of relative velocity normal to the sheet is zero, the velocity difference across the sheet, Δq , lies in the tangent plane to the sheet and hence can be written as

$$\Delta\underline{q} = \lambda\underline{a} + \mu\underline{b}$$

where λ and μ are scalar quantities. Taking the scalar product of this equation with $\underline{a}$ and $\underline{b}$ in turn we may calculate λ and we find that

$$\lambda\left(1 - (\underline{a} \cdot \underline{b})^2\right) = \underline{a} \cdot \Delta\underline{q} - (\underline{a} \cdot \underline{b})(\underline{b} \cdot \Delta\underline{q}) \quad .$$

Hence, since $\underline{i} \cdot \underline{b} = 0$

$$\Delta q_\xi = \underline{i} \cdot \Delta\underline{q} = \lambda \underline{i} \cdot \underline{a}$$

$$= \left(\underline{a} \cdot \Delta\underline{q} - (\underline{a} \cdot \underline{b})(\underline{b} \cdot \Delta\underline{q})\right)(\underline{i} \cdot \underline{a})/\left(1 - (\underline{a} \cdot \underline{b})^2\right) \quad . \tag{27}$$

Now, from (17)

$$\underline{a} \cdot \underline{q}_1 = \underline{a} \cdot (\underline{u}_1 - \underline{\Omega} \wedge \underline{r}) = \frac{1}{h_\xi} \frac{\partial \Phi_1}{\partial \xi} - \underline{a} \cdot (\underline{\Omega} \wedge \underline{r}) \tag{28}$$

where $h_\xi d\xi$ is the arc length along the curve η = constant on Σ and the partial derivative is for constant η on Σ. This expression differs from that found by Smith[14] for the steady potential flow case by the term which involves the vector $\underline{\Omega}$ explicitly. However, when we take differences across the vortex sheet these terms, being functions of position only, disappear and we have, from (28)

$$\underline{a} \cdot \Delta\underline{q} = \frac{1}{h_\xi}\left(\frac{\partial \Phi_1}{\partial \xi} - \frac{\partial \Phi_2}{\partial \xi}\right) = \frac{1}{h_\xi} \frac{\partial \Delta\Phi}{\partial \xi} \tag{29}$$

since the differentiation $\partial/\partial\xi$ is along a curve lying in the vortex sheet Σ. Here $\Delta\Phi$ is the circulation or the jump in potential across the vortex sheet. In a similar manner, from (23)

$$\Delta q_t = \underline{b} \cdot \Delta\underline{q} = \frac{1}{h_\eta} \frac{\partial \Delta\Phi}{\partial \eta} \tag{30}$$

where $h_\eta d\eta$ is the arc length along the curve ξ = constant on Σ. Substituting (29) and (30) into (27) and using the resulting equation for Δq_ξ in (26), we obtain for the pressure condition:

$$\frac{1}{h_\xi} \frac{\partial \Delta\Phi}{\partial \xi} = \Delta q_t \left(\underline{a} \cdot \underline{b} - \frac{q_{tm}}{U} \frac{1 - (\underline{a} \cdot \underline{b})^2}{\underline{i} \cdot \underline{a}}\right) \quad . \tag{31}$$

The two conditions (25) and (31) are the same as those derived by Smith[14] except that the actual velocities are replaced by the velocities relative to the rotating frame. In his paper Smith went on to express these conditions for a set of polar coordinates but in the present work we choose to express them in a different set of coordinates. Barsby[5] has shown that an intrinsic coordinate system is better able to handle the shapes of leading-edge vortex sheets that are encountered at low incidences. For this reason the coordinates ξ, η and ψ are chosen in the following way. ξ is identified with x, the coordinate measured in the downstream direction, so that $h_\xi = 1$. η is defined by

$$\eta = \frac{\sigma}{\ell} \quad , \tag{32}$$

where σ is the arc length along the sheet measured in the plane x = constant, and ℓ is an arbitrary function of x. We should like to keep the angle in the cross-flow plane which the line joining the isolated vortex to the free end of the vortex sheet makes with the wing approximately constant, and to generate this vortex sheet by a fixed range of values of η. To achieve this we choose ℓ to increase with x to keep pace with the growing size of the vortex system. ψ is the angle made by the tangent to the vortex sheet with some, as yet unspecified, reference line in the cross-flow plane. We also define a set of Cartesian axes (x, y, z) with y in the direction of $\psi = 0$ and with unit vectors $\underline{i}$, $\underline{j}$ and $\underline{k}$ in the direction of the axes.

In this case, in the expressions for the stream surface and pressure conditions (25) and (31) $\underline{i}$ is as we have just defined it, $\underline{a}$ is a unit vector in the tangent plane to Σ in the direction of η constant and x increasing, and $\underline{b}$ is a unit vector in the tangent plane with ψ constant and η increasing. These are sketched in Fig 3c. Thus

$$\underline{b} = \underline{j} \cos\psi + \underline{k} \sin\psi \tag{33}$$

and

$$\underline{a} = \frac{\underline{i} + \underline{j} \left.\frac{\partial y}{\partial x}\right|_\eta + \underline{k} \left.\frac{\partial z}{\partial x}\right|_\eta}{\sqrt{1 + \left(\left.\frac{\partial y}{\partial x}\right|_\eta\right)^2 + \left(\left.\frac{\partial z}{\partial x}\right|_\eta\right)^2}} \tag{34}$$

where $\left.\partial/\partial x\right|_\eta$ denotes the downstream derivative on the surface Σ, keeping η constant. By the slender-body assumptions:

$$\left(\frac{\partial y}{\partial x}\bigg|_\eta\right)^2 << 1 , \qquad \left(\frac{\partial z}{\partial x}\bigg|_\eta\right)^2 << 1$$

and hence, from (34):

$$\underline{a} = \underline{i} + \underline{j}\,\frac{\partial y}{\partial x}\bigg|_\eta + \underline{k}\,\frac{\partial z}{\partial x}\bigg|_\eta . \tag{35}$$

Since σ is the arc length in the direction of η increasing, $h_\eta d\eta = d\sigma$ and so, by (30);

$$\Delta q_t = \frac{\partial \Delta\Phi}{\partial \sigma} .$$

Using this, and equations (33) and (35), we obtain from (25) and (31) the stream surface and pressure conditions in the forms:

$$\frac{q_n}{U} = -\sin\psi\,\frac{\partial y}{\partial x}\bigg|_\eta + \cos\psi\,\frac{\partial z}{\partial x}\bigg|_\eta \tag{36}$$

and

$$\frac{\partial \Delta\Phi}{\partial x}\bigg|_\eta = \frac{\partial \Delta\Phi}{\partial \sigma}\left(\cos\psi\,\frac{\partial y}{\partial x}\bigg|_\eta + \sin\psi\,\frac{\partial z}{\partial x}\bigg|_\eta - \frac{q_{tm}}{U}\right). \tag{37}$$

These equations will also be applicable to the steady potential flow case, in which the velocities relative to the sheet in the cross-flow plane, q_{tm} and q_n, become the actual velocities $(\partial\Phi/\partial\sigma)_m$ and $\partial\Phi/\partial n$. Thus in this intrinsic coordinate system the relevant boundary conditions for a steady potential flow, for example a wing at incidence, are

$$\frac{1}{U}\frac{\partial \Phi}{\partial n} = -\sin\psi\,\frac{\partial y}{\partial x}\bigg|_\eta + \cos\psi\,\frac{\partial z}{\partial x}\bigg|_\eta \tag{38}$$

and

$$\frac{\partial \Delta\Phi}{\partial x}\bigg|_\eta = \frac{\partial \Delta\Phi}{\partial \sigma}\left(\cos\psi\,\frac{\partial y}{\partial x}\bigg|_\eta + \sin\psi\,\frac{\partial z}{\partial x}\bigg|_\eta - \frac{1}{U}\left(\frac{\partial \Phi}{\partial \sigma}\right)_m\right) . \tag{39}$$

For conical flow, if we choose c to be the wing semi-span so that the vortex sheet may grow linearly, we have

$$\left.\frac{\partial y}{\partial x}\right|_{\eta} = \tan\gamma\,\frac{y}{s}$$

$$\left.\frac{\partial z}{\partial x}\right|_{\eta} = \tan\gamma\,\frac{z}{s}$$

and

$$\frac{\partial \Delta\Phi}{\partial x} = \tan\gamma\,\frac{\Delta\Phi}{s}$$

where s is the semi-span of the delta wing and γ is the wing semi-apex angle. Hence, the conditions (38) and (39) become

$$\frac{\partial \Phi}{\partial n} = -\frac{U\tan\gamma}{s}(y\sin\psi - z\cos\psi) \tag{40}$$

and

$$\Delta\Phi = \frac{\partial \Delta\Phi}{\partial \sigma}\left(y\cos\psi + z\sin\psi - \frac{s}{U\tan\gamma}\left(\frac{\partial\Phi}{\partial\sigma}\right)_m\right) . \tag{41}$$

If we finally consider a polar coordinate representation of the vortex sheet in the cross-flow plane, we have

$$r\cos\phi = y\cos\psi + z\sin\psi$$

and

$$r\sin\phi = y\sin\psi - z\cos\psi$$

where ϕ is the angle made by the radius vector with the tangent to the sheet. Then, from (40) and (41) we have

$$\Phi_n = -\frac{U\tan\gamma\, r\sin\phi}{s}$$

and

$$\Lambda\Phi = \frac{\partial\Delta\Phi}{\partial\sigma}\left(r\cos\phi - \frac{s}{U\tan\gamma}\left(\frac{\partial\Phi}{\partial\sigma}\right)_m\right) ,$$

which are the usual conditions for a conical flow[3].

4 THE EQUATIONS GOVERNING THE SEPARATED FLOW

In the two preceding sections we have obtained an expression for the complex potential of the attached flow in section 2 and derived convenient forms for

the boundary conditions to be applied on the vortex sheet in section 3. In this section we add terms representing the leading-edge vortices to the attached flow potential to obtain a complete description of the separated flow field; and we formulate the remaining conditions which this flow field must satisfy, the Kutta condition at the leading edge and the vanishing of the force acting on the coordinates of the isolated vortex and cut. Finally the complete system of equations is presented in a non-dimensional form based upon the radius r of the cylindrical body and the free stream speed U.

4.1 Complex potential for separated flow

As described in the Introduction the fully rolled-up vortex sheet of infinite extent which is sketched below the port wing in Fig 1 is replaced by a finite length of vortex sheet, an isolated vortex filament and a cut connecting these, as illustrated above the starboard wing in Fig 1. The configuration to be represented has central symmetry about the axis of the cylinder, so that it is sufficient to specify the shape and strength of the vortex system in the first quadrant.

In section 2 we found expressions for the complex potential (12) and its derivative (13) at time $t = 0$ which satisfy the boundary conditions on the cross-section of wing-body combination and at infinity and which are analytic on the cross-flow plane outside the cross-section. We now wish to add terms which have an appropriate singular behaviour on the sections of the vortex sheets and at the positions of the vortex filaments and which do not disturb the boundary conditions on the wing-body combination and at infinity. This is easily achieved by using the conformal transformation (4) of the cross-flow plane of Fig 1 onto the ζ-plane of Fig 2. The wing-body contour becomes the unit circle in the ζ-plane and so the boundary condition on the contour is preserved by including the image inside the circle of every singularity introduced outside it. The boundary condition is also preserved if a vortex of arbitrary strength is added at the centre of the circle in the ζ-plane. However, since the total circulation of each element of vorticity in the flow field and its image inside the circle is zero, a vortex at the centre of the circle represents a net circulation about the cross-section of the configuration. No such circulation can exist, since any contour surrounding the cross-section can be displaced upstream, following streamlines, into the undisturbed flow. Hence no vortex should exist at the centre of the circle.

The required velocity in the cross-flow plane is then the complex conjugate of:

$$\frac{\partial W}{\partial \zeta} = \frac{\partial W_A}{\partial \zeta} + \frac{\Gamma}{2\pi i}\left\{\frac{1}{\zeta - \zeta_v} - \frac{1}{\zeta - \frac{1}{\bar{\zeta}_v}} + \frac{1}{\zeta + \zeta_v} - \frac{1}{\zeta + \frac{1}{\bar{\zeta}_v}}\right\}$$

$$+ \int_0^{\sigma_E}\left(-\frac{1}{2\pi i}\frac{\partial \Delta\Phi}{\partial \sigma}\right)\left\{\frac{1}{\zeta - \zeta(\sigma)} - \frac{1}{\zeta - \frac{1}{\bar{\zeta}(\sigma)}} + \frac{1}{\zeta + \zeta(\sigma)} - \frac{1}{\zeta + \frac{1}{\bar{\zeta}(\sigma)}}\right\} d\sigma \quad (42)$$

where $\partial W_A/\partial \zeta$ is given by (13). Γ is the circulation of the isolated vortex filament in the first quadrant, this vortex lying at the point ζ_v in the ζ-plane. The arc length along the vortex sheet in the first quadrant in the physical plane, σ, is used as the integration variable and takes the value σ_E at the free end of the sheet, $\Delta\Phi$ is the jump in potential across the sheet and the minus sign arises because $\Delta\Phi$ decreases as σ increases, and $\zeta(\sigma)$ is the position of a current point of the starboard sheet on the ζ-plane. The successive terms in each curly bracket in (42) arise from the starboard singularity, its image in the unit circle, the port singularity and its image in the circle.

4.2 Conditions on the separated flow field

The construction of relation (42) ensures that the boundary conditions on the wing-body and at infinity are satisfied. The boundary condition on the vortex sheets (and as pointed out above, it is enough to consider one sheet) are given by equations (36) and (37), in terms of the velocity $\underline{q}$ relative to the rotating frame of reference in which the flow is steady, but rotational. $\underline{q}$ is related to the irrotational velocity field $\underline{u}$ of the unsteady potential flow at time $t = 0$ by equation (17). Taking components of (17) along the tangent and normal to the cross-section of the sheet we have

$$q_{tm} = \left(\frac{\partial \Phi}{\partial \sigma}\right)_m - \Omega y \sin\psi + \Omega z \cos\psi$$

$$q_n = \frac{\partial \Phi}{\partial n} - \Omega y \cos\psi - \Omega z \sin\psi \quad .$$

Combining these two into a single complex equation we have

$$q_{tm} - iq_n = \frac{\partial W}{\partial \sigma} + i\Omega\bar{Z}e^{i\psi}$$

$$= \left(\frac{\partial W}{\partial Z} + i\Omega\bar{Z}\right)e^{i\psi} \quad (43)$$

since $\frac{\partial Z}{\partial \sigma} = e^{i\psi}$.

Integrating this last equation gives a convenient expression for the coordinates of the sheet in the physical plane:

$$Z = s(x) + \int_0^{\sigma} e^{i\psi} d\sigma \quad . \tag{44}$$

The Kutta condition at the leading edge requires that the velocity there is finite. Since in the transformation (4) the leading edge, $Z = s$, at which $\zeta = 1$, is a singular point at which $\partial Z/\partial \zeta$ vanishes, the Kutta condition implies that

$$\frac{\partial W}{\partial \zeta} = 0 \qquad \text{at } \zeta = 1 \quad . \tag{45}$$

We now consider the forces acting on the cut and on the isolated vortex filament. The difference in pressure across the cut, inside minus outside, is given by (14) as

$$\Delta p = \rho \Delta \left(- \frac{\partial \Phi}{\partial t} - \tfrac{1}{2} \underline{u} \cdot \underline{u} \right) .$$

Equation (19) expresses $\partial \Phi / \partial t$ in terms of the cross-flow velocities and these are continuous across the cut. Hence, neglecting $(\partial \Phi / \partial x)^2$, the pressure jump becomes

$$\Delta p = - \rho U \Delta \frac{\partial \Phi}{\partial x} = - \rho U \frac{d\Gamma}{dx} \quad ,$$

since the jump in potential across the cut is just the circulation about the vortex filament. The force on the section of the cut between two cross-flow planes a small distance Δx apart produced by this pressure difference is given in magnitude and direction by

$$- i(Z_V - Z_E) \Delta p \Delta x = i \rho U (Z_V - Z_E) \frac{d\Gamma}{dx} \Delta x \quad , \tag{46}$$

where Z_V and Z_E are the position of the vortex filament and the free end of the vortex sheet.

Randall[13] has shown that the force on an element of a vortex filament of length Δx in an unsteady potential flow is given by the classical Joukowski formula for steady flow, viz:

$$- i\rho\Gamma\underline{Q}\Delta x$$

where $\underline{Q}$ is the complex velocity normal to the vortex element. In the present situation there are three contributions to $\underline{Q}$. One comes from the unsteady potential flow in the cross-flow plane and is obtained by deducting the influence of the vortex itself from the complete cross-flow velocity, giving

$$\underline{Q}_1 = \lim_{Z \to Z_V} \left\{ \overline{\frac{\partial W}{\partial Z} - \frac{\Gamma}{2\pi i (Z - Z_V)}} \right\}$$

where the bar denotes the complex conjugate. The second contribution comes from the relative velocity between the rotating and inertial frames, given from (17) as

$$\underline{Q}_2 = - i\Omega Z_V \quad .$$

The third contribution comes the inclination of the vortex filament to the free stream, viz:

$$\underline{Q}_3 = - U \frac{dZ_V}{dx} \quad .$$

Writing $\underline{Q} = \underline{Q}_1 + \underline{Q}_2 + \underline{Q}_3$, and equating to zero the sum of the force on the element of the vortex and force (46) on the element of the cut, we obtain

$$(Z_V - Z_E) \frac{d\Gamma}{dx} - \frac{\Gamma}{U} \lim_{Z \to Z_V} \left(\overline{\frac{\partial W}{\partial Z} - \frac{\Gamma}{2\pi i (Z - Z_V)}} \right) + \frac{i\Omega Z_V \Gamma}{U} + \frac{\Gamma dZ_V}{dx} = 0 \quad . \qquad (47)$$

This is the final condition to be imposed on the vortex system.

4.3 Non-dimensional form of the equations

We define a non-dimensional parameter P to describe the rate of roll

$$P = - \frac{r\Omega}{U} \quad . \qquad (48)$$

The minus sign is introduced so that we have a vortex sheet in the first quadrant, as in Fig 1, where P is positive. If the configuration is regarded as moving forward with speed U, the apex A of the exposed wing describes a helix whose inclination to its axis is $\tan^{-1} P$.

Since the body radius r is independent of x, it is convenient to use it as a length scale, with the free stream velocity U as a velocity scale. From this point on, *the same symbols as before will be used, but they will be used for the quantities made dimensionless in this way.*

In non-dimensional form then the stream-surface condition (36) and pressure condition (37) become

$$q_n = -\sin\psi \left.\frac{\partial y}{\partial x}\right|_\eta + \cos\psi \left.\frac{\partial z}{\partial x}\right|_\eta \tag{49}$$

and

$$\left.\frac{\partial \Delta\Phi}{\partial x}\right|_\eta = \frac{\partial \Delta\zeta}{\partial \sigma}\left(\cos\psi \left.\frac{\partial y}{\partial x}\right|_\eta + \sin\psi \left.\frac{\partial z}{\partial x}\right|_\eta - q_{tm}\right) \tag{50}$$

where now, from (43) and (48)

$$q_{tm} - iq_n = \left(\frac{\partial W}{\partial \zeta}\frac{\partial \zeta}{\partial Z} - iP\bar{Z}\right)e^{i\psi} \quad . \tag{51}$$

The force condition (47) becomes

$$(Z_V - Z_E)\frac{d\Gamma}{dx} + \Gamma\frac{dZ_V}{dx} - iPZ_V - \lim_{Z\to Z_V} \Gamma\left[\overline{\frac{dW}{dZ} - \frac{\Gamma}{2\pi i(Z - Z_V)}}\right] = 0 \tag{52}$$

and the Kutta condition (45) remains as

$$\frac{\partial W}{\partial \zeta} = 0 \quad \text{at } \zeta = 1 \quad . \tag{53}$$

The complex conjugate of the attached-flow velocity (13) is now given by

$$\frac{\partial W_A}{\partial \zeta} = P\left\{\frac{2i \sin 2\theta_1}{\pi\zeta\left(\zeta^2 + \frac{1}{\zeta^2} - 2\cos 2\theta_1\right)} - \frac{i\theta_1\left(\zeta^2 + \frac{1}{\zeta^2}\right)}{\zeta\pi \cos^2\theta_1}\right.$$

$$+ \frac{1}{2}\frac{\left(\zeta^2 - \frac{1}{\zeta^2}\right)}{\pi \cos^2\theta_1 \zeta} \log\left\{\frac{(\zeta^2 - 1) + i \tan\theta_1(\zeta^2 + 1)}{(\zeta^2 - 1) - i \tan\theta_1(\zeta^2 + 1)}\right\}$$

$$- \frac{4 i \tan\theta_1}{\pi \cos^2\theta_1}\left\{\frac{1}{2}\left(\zeta^2 + \frac{1}{\zeta^2}\right) + \sin^2\theta_1\right\}\frac{\zeta}{\left((\zeta^2 - 1)^2 + \tan^2\theta_1(\zeta^2 + 1)^2\right)}$$

$$\left. - \frac{\left(\zeta^2 + \frac{1}{\zeta^2}\right)}{2\cos^2\theta_1} - \frac{i\sqrt{\zeta^4 - 2\cos 2\theta_1 \zeta^2 + 1}}{2\cos^2\theta_1 \zeta^3} + \frac{i(\zeta^2 + 1)}{2\cos^2\theta_1}\frac{1}{\zeta}\frac{(\zeta^2 - \cos 2\theta_1)}{\sqrt{\zeta^4 - 2\cos 2\theta_1 \zeta^2 + 1}}\right\}$$

and the complex conjugate of the velocity of the separated flow (42) is

$$\frac{\partial W}{\partial \zeta} = \frac{\partial W_A}{\partial \zeta} + \frac{\Gamma}{2\pi i}\left\{\frac{1}{\zeta - \zeta_v} - \frac{\bar{\zeta}_v}{\zeta\bar{\zeta}_v - 1} + \frac{1}{\zeta + \zeta_v} - \frac{\bar{\zeta}_v}{\zeta\bar{\zeta}_v + 1}\right\}$$

$$+ \int_0^{\sigma_E} - \frac{1}{2\pi i}\frac{\partial \Lambda\Phi}{\partial \sigma}\left\{\frac{1}{\zeta - \zeta(\sigma)} - \frac{\bar{\zeta}(\sigma)}{\zeta\bar{\zeta}(\sigma) - 1} + \frac{1}{\zeta + \zeta(\sigma)} - \frac{\bar{\zeta}(\sigma)}{\zeta\bar{\zeta}(\sigma) + 1}\right\}$$

.....(54)

The formula for the sheet coordinates (44) remains unaltered in non-dimensional form and so the relationship between (y, z) and (ψ, σ) may be written, as before,

$$Z = s(x) + \int_0^{\sigma} e^{i\psi} d\sigma \quad . \tag{55}$$

With the complex velocity in the transformed cross-flow plane now given by (54) the equations which express the boundary conditions, namely (49), (50), (52) and (53), and so determine the position and strengths of the isolated vortices and vortex sheets, may be reduced to a set of nonlinear ordinary differential equations in the streamwise variable x. Since the flow near the apex of each exposed wing panel is approximately conical, initial values of the unknowns are available from previous solutions, and the equations can be solved using a marching procedure. This procedure is described in the following section.

For a given combination of a slender wing on a cylindrical body, for a specific non-dimensional local semi-span $s(x)$, the solution depends only on the parameter P defining the rate of roll.

5 FINITE DIFFERENCE FORMULATION AND SOLUTION PROCEDURE

The finite difference formulation that we use to solve the nonlinear differential equations derived from expressing the boundary conditions as in section 4 can be split into two separate parts. The first is the discretization in the streamwise direction. The second concerns the numerical representation of the vortex system in each cross-flow plane and the solution of the resulting equations for each cross-flow plane.

In the finite difference representation that we adopt the shape of the sheet in each cross-flow plane is defined by the value of the angle ψ at n points on it, with the sheet strength defined by $-\partial\Delta\Phi/\partial\sigma$, again evaluated at the same points. These points are mid-points of specially chosen intervals and for this reason they are known as intermediate points. The intervals are defined later. The values which represent the strength and shape of each sheet, together with the real and imaginary parts of the position Z_V, and the strength Γ, of the corresponding isolated vortex give $2n + 3$ unknowns represented by the vector $\underline{X}$, say, to be determined in each cross-flow plane.

Near its apex, the exposed wing is small relative to the body, so that the body can be approximated by a vertical plane, and the exposed wing reflected in this plane forms a delta wing. This 'delta wing' may now be thought of as a fixed wing at incidence. Since it is moving downwards with velocity $-r_c$ in dimensional form and the oncoming flow has velocity U, the situation is equivalent to a wing in a flow at an angle of incidence $\alpha = -r_c/U$, which is equal to the roll rate parameter P defined in the previous section. Hence an available conical flow solution will give the unknowns $\underline{X}(x_0)$ in the cross-flow plane $x = x_0$, say, where x_0 is sufficiently small.

With the initial solution $\underline{X}(x_0)$ known, we use a marching procedure based on the Crank-Nicolson method for advancing the solution through successive cross-flow planes $x_{m+1} = x_m + h_x$, $m = 0, 1, 2, \ldots$, where h_x is the step length in the downstream direction. At each step our objective is to satisfy in some cross-flow plane, the stream surface and pressure conditions (49) and (50) at the intermediate points on the sheet, the two components of the force condition (52), and the Kutta condition (53) at the leading edge, giving $2n + 3$ equations to solve for the $2n + 3$ unknown components of $\underline{X}(x_{m+1})$. These equations are solved by an iterative method described in detail later. The method starts from a guess at the solution vector $\underline{X}(x_{m+1})$ and uses the residuals (*ie* the differences between the left- and right-hand sides) of equations (49), (50), (52) and (53) to improve on this guess. The solution at $x = x_0$ is simply the conical solution and further downstream linear extrapolation from the two previous cross-flow planes is used to generate an initial guess.

We first describe how the quantities appearing in (49), (50), (52) and (53) are calculated at $x = x_m + h_x/2$ from the known solution vector $\underline{X}(x_m)$ and a guess at the solution vector $\underline{X}(x_{m+1})$. The streamwise derivatives are approximated by central-difference formulae:

$$\frac{\partial}{\partial x} f(x_m + h_x/2, \eta) = \frac{f(x_m + h_x, \eta) - f(x_m, \eta)}{h_x} + O\left(h_x^2\right) . \qquad (56)$$

For the remaining terms, linear interpolation is used to provide an approximation to $\underline{X}(x_m + h_x/2)$:

$$\underline{X}(x_m + h_x/2) = \tfrac{1}{2}[\underline{X}(x_m) + \underline{X}(x_{m+1})] + O\left(h_x^2\right) , \qquad (57)$$

and from this we proceed to evaluate the quantities needed in the cross-flow plane $x = x_m + h_x/2$.

As indicated earlier we use an intrinsic coordinate system (η, ψ) where η is defined in equation (32), to represent the sheet shape in each cross-flow plane. In discretizing the sheet itself in the cross-flow plane we require, in particular, an accurate representation of the sheet near the leading edge of the wing where its shape changes most rapidly. To achieve this we define a new variable τ such that

$$\eta = \frac{\sigma}{\ell} = \frac{\lambda \tau^2 (7 - \tau)}{6(1 + \tau)} \qquad (58)$$

where ϱ is the quantity introduced in section 3 and λ is a constant chosen to give the required angular extent of the sheet at the initial station. In the results presented in the next section λ is chosen so that at the initial station the angle made by the radius vector from the isolated vortex to the free end of the sheet with the real axis is 2 radians, and ϱ is given by (68).

The formula for the sheet coordinates (55) now becomes

$$Z = s - \int_0^{\tau} e^{i\psi} \varrho \frac{d\eta}{d\tau} d\tau \quad . \tag{59}$$

We now define $n + 1$ pivotal points to be equally spaced in τ, with step length h_τ, say, and the leading edge chosen as the first pivotal point. Throughout the calculations we have set $h_\tau = 0.1$. Similarly n intermediate points are defined with the same spacing in τ but commencing at the point $\tau = h_\tau/2$. The representation (58) of arc length was introduced by Barsby[28]; it gives $\eta \sim 7\lambda\tau^2/6$ near the leading edge and the quadratic dependence upon τ ensures an adequate density for the pivotal and intermediate points close to the leading edge. Also the intermediate points in successive cross-flow planes are defined by constant values of τ and (58) then ensures that η is constant for these points as is required in the definition of the streamwise derivatives on the sheet.

It is convenient at this stage to adopt a numbering system for the quantities evaluated at the pivotal and intermediate points, such that to the pivotal points are assigned odd numbered subscripts and to the intermediate points even numbered subscripts. Thus, for example, η_{2j} refers to η evaluated at the jth intermediate points and η_{2j-1} refers to η evaluated at the jth pivotal point.

From $\underline{X}(x_m + h_x/2)$ we know the values of ψ at the jth intermediate point, ψ_{2j}, $j = 1(1)n$, and using these values we may calculate ψ_{2j-1}, $j = 1(1)n+1$, the values of ψ at the pivotal points. Because the sheet must leave the wing tangentially we have $\psi_1 = 0$ and the remainder are found using four point Lagrangian interpolation formulae. Thus

$$\left.\begin{aligned}
\psi_3 &= (-4\psi_1 + 15\psi_2 + 10\psi_4 - \psi_6)/20 \quad , \\
\psi_{2j-1} &= (-\psi_{2j-4} + 9\psi_{2j-2} + 9\psi_{2j} - \psi_{2j+2})/16 \quad , \qquad j = 3(1)n-1 \quad , \\
\psi_{2n-1} &= (\psi_{2n-6} - 5\psi_{2n-4} + 15\psi_{2n-2} + 5\psi_{2n})/16 \\
\text{and} \\
\psi_{2n+1} &= (-5\psi_{2n-6} + 21\psi_{2n-4} - 35\psi_{2n-2} + 35\psi_{2n})/16 \quad .
\end{aligned}\right\} \quad (60)$$

The sheet coordinates at the pivotal points, Z_{2n-1} , $j = 1(1)n+1$, may now be calculated from (59) using Simpson's rule to achieve comparable accuracy with the interpolation formulae (60). Thus

$$Z_1 = s$$

and

$$Z_{2j+1} = Z_{2j-1} + \frac{h_\tau \ell}{6}\left[e^{i\psi_{2j-1}}\eta'_{2j-1} + 4e^{i\psi_{2j}}\eta'_{2j} + e^{i\psi_{2j+1}}\eta'_{2j+1}\right] , j = 1(1)n , \quad (61)$$

where the prime denotes a derivative with respect to τ . To calculate the coordinates of the intermediate points, Z_{2j}, $j = 1(1)n$, we must first evaluate

$$Z_2 = Z_1 + \frac{h_\tau \ell}{48}\left[9e^{i\psi_1}\eta'_1 + 19e^{i\psi_2}\eta'_2 - 5e^{i\psi_3}\eta'_3 + e^{i\psi_4}\eta'_4\right] . \quad (62)$$

This formula has the same order of accuracy as Simpson's rule. We may then evaluate the positions of the remaining intermediate points using Simpson's rule in a manner similar to that for the pivotal points. Hence

$$Z_{2j} = Z_{2j-2} + \frac{h_\tau}{6}\left[e^{i\psi_{2j-2}}\eta'_{2j-2} + 4e^{i\psi_{2j-1}}\eta'_{2j-1} + e^{i\psi_{2j}}\eta'_{2j}\right] , \quad j = 2(1)n \quad .$$

The sheet strength is specified in terms of the parameters ζ_j , where

$$g_j = -\left(\frac{\partial \Delta\Phi}{\partial \tau}\right)_\gamma = -\left(\frac{\partial \Delta\Phi}{\partial \sigma}\frac{\partial \sigma}{\partial \tau}\right)_\gamma \qquad j = 1(1)2n+1 \quad .$$

The values at the pivotal and intermediate points are related by equations like (60) for the angles ψ . To calculate the sheet circulation at the intermediate points we have

$$\Delta\Phi = \Gamma + \int_{\sigma}^{\sigma_E} -\frac{\partial\Delta\Phi}{\partial\sigma}\, d\sigma \ .$$

To evaluate this we adopt a procedure similar to that which gives Z_{2j} at the intermediate points. Thus we first evaluate the circulation at the last intermediate point using an integration formula analogous to (62), and for the other intermediate points we add on the contribution from the rest of the integral which is calculated using Simpson's rule. The circulation at the intermediate points is then given by

$$\Delta\Phi_{2n} = \Gamma + \frac{h_1}{48}\left[9g_{2n+1} + 19g_{2n} - 5g_{2n-1} + g_{2n-2}\right]$$

and

$$\Delta\Phi_{2j} = \Delta\Phi_{2j+2} + \frac{h_1}{6}\left[g_{2j} + 4g_{2j+1} + g_{2j+2}\right], \quad j = n-1(-1)1 \ .$$

The sheet coordinates in the transformed plane ζ_j, $j = 1(1)2n+1$, are calculated from the corresponding coordinates in the cross-flow plane using equation (4). Hence, in non-dimensional form

$$\zeta_j = Z^*_j + \sqrt{Z^{*2}_j - 1}$$

where

$$Z^*_j = (Z_j + 1/Z_j)s/(1 + s^2) \ . \qquad (63)$$

Because the sheet with which we are concerned lies entirely in the first quadrant, the branch of the square root with positive imaginary part is used.

To calculate the complex velocity dW/dz at any point ζ in the transformed plane we must evaluate the integral in equation (54) numerically. This must be considered for three separate cases:

(i) when the point ζ is not on the sheet, as in the force condition, Simpson's rule can be used immediately since the integrand is non-singular everywhere.

(ii) When $\zeta = 1$, as in the Kutta condition, the integrand is singular at $\sigma = 0$, where $\zeta(\sigma) = \bar{\zeta}(\sigma) = 1$. We show that the singularity is integrable and obtain a numerical procedure for evaluating the integral. We note first that the

last two terms in the bracket under the integral sign in (54) cancel at $\sigma = 0$ when $\zeta = 1$. To examine the behaviour of the first two terms, we recall that the sheet leaves the wing tangentially, so that, for points on a sheet close to the leading edge

$$Z \sim s + \sigma .$$

Hence, by (4) or (63),

$$\zeta(\sigma) \sim 1 + \left(\frac{2(s^2 - 1)\sigma}{s(s^2 + 1)}\right)^{\frac{1}{2}} \quad \text{and} \quad \bar{\zeta}(\sigma) \sim \zeta(\sigma) .$$

Hence, for $\zeta = 1$, the first two terms in the bracket in (54) are

$$\frac{1}{1 - \zeta(\sigma)} - \frac{\bar{\zeta}(\sigma)}{\bar{\zeta}(\sigma) - 1} \sim \left(\frac{2s(s^2 + 1)}{(s^2 - 1)\sigma}\right)^{\frac{1}{2}} .$$

Since $\partial\Delta\Phi/\partial\sigma$ is finite at the leading edge, by the Kutta condition, this shows that the singularity at $\sigma = 0$ is integrable. To remove the singularity, we change the variable of integration to τ. By (58)

$$\sigma \sim 7\lambda\ell\tau^2/6$$

and so

$$\left(\frac{1}{1 - \zeta(\sigma)} - \frac{\bar{\zeta}(\sigma)}{\bar{\zeta}(\sigma) - 1}\right) d\sigma \sim 2\left(\frac{7\lambda\ell s(s^2 + 1)}{3(s^2 - 1)}\right)^{\frac{1}{2}} d\tau . \qquad (64)$$

With τ as variable of integration, the integrand is therefore regular and Simpson's rule can again be used. The value of the integrand at $\tau = 0$ is given by combining (64) with a four-point Lagrangian extrapolation formula for $\partial\Delta\Phi/\partial\sigma$:

$$\left(\frac{\partial\Delta\Phi}{\partial\sigma}\right)_{\tau=0} = \frac{1}{16}\left(35\left(\frac{\partial\Delta\Phi}{\partial\sigma}\right)_1 - 35\left(\frac{\partial\Delta\Phi}{\partial\sigma}\right)_3 + 21\left(\frac{\partial\Delta\Phi}{\partial\sigma}\right)_5 - 5\left(\frac{\partial\Delta\Phi}{\partial\sigma}\right)_7\right) . \qquad (65)$$

(iii) When $\partial W/\partial\zeta$ is evaluated at $\zeta = \zeta_0$ on the vortex sheet, in order to calculate q_{tm} and q_n from (51), the integrand is singular and the integral must be regarded as a Cauchy principal value. The singular behaviour arises from the first term in the bracket of (54) and is dealt with as follows:

$$\int_0^{\sigma_E} \frac{\partial \Delta\Phi}{\partial \sigma} \frac{d\sigma}{\zeta_0 - \zeta(\sigma)} = \int_0^{\sigma_E} \left(\frac{\partial \Delta\Phi}{\partial \sigma} - \left.\frac{\partial \Delta\Phi}{\partial \sigma}\right|_{\zeta_0} \right) \frac{d\sigma}{\zeta_0 - \zeta(\sigma)} + \left.\frac{\partial \Delta\Phi}{\partial \sigma}\right|_{\zeta_0} \left.\frac{\partial \sigma}{\partial \zeta}\right|_{\zeta_0} \int_1^{\zeta_E} \frac{d\zeta}{\zeta_0 - \zeta} \quad ,$$

where $\zeta_E = \zeta(\sigma_E)$ and the partial derivative signs merely indicate that x is constant. The first term on the right is regular and the integral in the second can be evaluated analytically as a Cauchy principal value:

$$\int_1^{\zeta_E} \frac{d\zeta}{\zeta_0 - \zeta} = \ln \frac{\zeta_0 - 1}{\zeta_E - \zeta_0} \quad .$$

Consideration of the simple case in which the sheet lies along the real axis and $1 < \zeta_0 < \zeta_E$, for which the integral should be real, shows that the imaginary part of the logarithm must be non-negative and less than 2π.

Finally in the numerical formulation of the problem we need to evaluate the limit in equation (52) expressing the force condition. The only term in (54) for $\partial W/\partial z$ which gives rise to a singularity in $\partial W/\partial Z$ is $\Gamma/2\pi i(\zeta - \zeta_v)$, so we need only consider the limit of

$$\frac{1}{\zeta - \zeta_v} \frac{\partial \zeta}{\partial Z} - \frac{1}{Z - Z_v} = \frac{\partial}{\partial Z} \ln \frac{\zeta - \zeta_v}{Z - Z_v}$$

as Z tends to Z_v. Expanding $\zeta - \zeta_v$ in a Taylor series gives

$$\ln \frac{\zeta - \zeta_v}{Z - Z_v} \quad \ln \left.\frac{\partial \zeta}{\partial Z}\right|_v + (Z - Z_v) \left.\frac{\partial^2 \zeta}{\partial Z^2}\right|_v \Bigg/ 2 \left.\frac{\partial \zeta}{\partial Z}\right|_v + O(Z - Z_v)^2 \quad .$$

Hence

$$\lim_{Z \to Z_v} \left\{ \frac{1}{\zeta - \zeta_v} \frac{\partial \zeta}{\partial Z} - \frac{1}{Z - Z_v} \right\} = \left(\frac{\partial^2 \zeta}{\partial Z^2} \Bigg/ 2 \frac{\partial \zeta}{\partial Z} \right)_v$$

$$= \frac{1}{2} \left(\frac{\partial}{\partial Z} \ln \frac{\partial \zeta}{\partial Z} \right)_v$$

$$= \frac{1}{Z_v(Z_v^2 - 1)} - \frac{1}{\zeta_v(\zeta_v^2 - 1)} \left.\frac{\partial \zeta}{\partial Z}\right|_v \qquad (66)$$

since

$$\frac{\partial \zeta}{\partial Z} = \frac{2s}{1+s^2}\,\frac{Z^2-1}{\zeta^2-1}\,\frac{\zeta^2}{Z^2} \quad , \qquad \text{by (4)} \ .$$

This completes the account of the numerical formulation of the equations governing the model and we now proceed to describe how they are solved.

We have explained how satisfying the discretized boundary conditions at $x = x_m + h_x/2$ gives rise to $2n + 3$ equations in the values taken by the $2n + 3$ unknowns, ψ_j, g_j, Γ and Z_v, at $x = x_{m+1}$. We have denoted the vector of these unknowns by $\underline{X}(x_{m+1})$. When a trial set of these unknowns is introduced into the set of $2n + 3$ equations, they generate $2n + 3$ residuals, each residual being the difference between the left- and right-hand sides of an equation. Let us denote the vector formed by these residuals by $\underline{F}\left(\underline{X}(x_{m+1})\right)$. Our object is to modify $\underline{X}$ so as to reduce $\underline{F}$ to zero. Note that neither the ordering of the unknowns in $\underline{X}$ nor that of the equations in $\underline{F}$ is significant.

If we have currently a vector $\underline{X}^r$ and the solution is $\underline{X}$, and $\underline{X}^r$ is close to $\underline{X}$ in some sense, we can use the multivariate form of the Taylor expansion to write

$$0 = \underline{F}(\underline{X}) \simeq \underline{F}(\underline{X}^r) + J \,.\, (\underline{X} - \underline{X}^r)$$

where J is the Jacobian matrix of the system, *ie* the matrix with $\partial F_i/\partial X_j$ in its ith row and jth column. If the sign of approximate equality is replaced by equality and the resulting equation is solved for $\underline{X}$, it is reasonable to expect that the solution will be closer (in an appropriate sense) to the true solution than $\underline{X}^r$ is, so it is taken as the next approximation $\underline{X}^{r+1}$:

$$\underline{X}^{r+1} = \underline{X}^r - J^{-1}\underline{F}(\underline{X}^r) \ . \qquad (67)$$

This is a straightforward multivariate extension of the Newton-Raphson procedure for the iterative solution of a single equation in one unknown. As in the single-variable case, convergence is quadratic if $\underline{X}^r$ is sufficiently close to the solution and J is calculated exactly. The success of this method however does not depend upon an accurate value for the Jacobian and it is calculated numerically from the initial approximation using the simple forward difference formula

$$\frac{\partial F_i}{\partial X_j} = \frac{F_i(X_1,\ldots,X_{j-1},X_j+\delta,X_{j+1},\ldots,X_k) - F_i(X_1,\ldots,X_j,\ldots,X_k)}{\delta}$$

where $k = 2n + 3$ and δ is a suitably chosen quantity for the evaluation of the derivatives. The numerical technique used for calculating $(\underline{X}^{r+1} - \underline{X}^{r})$ in (67) is based on Gaussian elimination. Basically one wishes to solve the set of linear equations

$$J\underline{X}^{*} = \underline{F} \ ,$$

where in this problem $\underline{X}^{*} = \underline{X}^{r} - \underline{X}^{r+1}$. To achieve this the matrix J may be written in the form

$$J = LU$$

where L and U are lower and upper triangular matrices respectively and we have

$$LU\underline{X}^{*} = \underline{F} \ .$$

This represents the two triangular systems

$$L\underline{Y} = \underline{F} \quad \text{and} \quad U\underline{X}^{*} = Y \ .$$

The first is solved for $\underline{Y}$ using forward substitution and the second solved using back substitution. This method for solving a set of linear equations is discussed in more detail in Forsythe and Moler[29]. Once the solution has been obtained for $\underline{X}(x_{m+1})$, that is when $\sqrt{\underline{F} \cdot \underline{F}} \leq 10^{-7}$, the numerical procedure continues marching downstream.

When using the solution procedure described above instabilities can be encountered in practice which manifest themselves as oscillations associated with successive downstream solutions. Ultimately the oscillations lead to a situation in which the procedure fails to converge. Numerical experiments indicate that the oscillations occur when the errors in the initial approximation which is adopted are significant in relation to the downstream step length. In the present work it is clear that the conical solution adopted as the starting solution is only an approximate solution, but that the approximation improves as x_0 decreases. However as x_0 decreases it is found that in order to maintain accuracy, and for the Newton iteration to converge, h_x must also decrease as the scale of the vortex system is diminishing. As a consequence it is difficult to avoid the instability. By contrast for the non-conical flows considered in (17) the starting solution was determined exactly as a conical solution and the instability did not occur.

To overcome the instability in the present case an averaging or smoothing technique is employed. This consists of finding the solution at $x = x_0 + h_x$ by

the technique described above and then calculating $\underline{X}(x_0 + h_x/2)$ from (57). This is then used as the initial solution to advance the solution to $x_0 + 3h_x/2$ and an averaged solution at $x_0 + h_x$ is found. This process is then continued downstream. This smoothing technique damps out any instability very effectively. However it has only the accuracy of a backward-difference scheme and therefore is less accurate by a factor of the order of h_x than the scheme which we have proposed above. We therefore choose $h_x = 0.01$, at most, when the smoothing technique is used to overcome potential instability, whereas much larger values of h_x may be used when the original scheme is employed. In this way the reduced accuracy of the smoothing technique is accommodated. The smoothing technique is used for the first few steps until it proves possible to obtain a converged solution for a larger step length, or until the errors associated with the approximate solution have been damped out. Thereafter the original full central-difference method is used.

As the solution is advanced downstream the number of iterations required at each step to obtain a solution decreases. The numerical procedure can then be speeded up considerably by only recalculating the Jacobian J and repeating the triangular decomposition at the start of the Newton iteration when the number of iterations required at the previous step is greater than some specified number. Typically it was recalculated when the number of iterations needed at each step was greater than 6 and it was by no means unusual, especially for large distances downstream, for the procedure to march for many steps before recalculating J.

6 RESULTS

6.1 Parameter values

We wish to compare results obtained by the present method, using slender-body theory for a wing-body combination, with Harvey's measurements[21] on a delta wing. (The present method is, of course, equally applicable to wings of any slender planform.) Regarding the delta wing within the context of slender-body theory, in which there is no upstream influence, we note that the only length-scale is the local semi-span $s_d(x)$. If, therefore, for two delta wings of the same apex angle, each rolling at zero incidence, there are cross-flow planes for which the values of $\Omega s_d(x)/U$ are the same, the flow fields in these planes will be the same, when scaled in terms of the length $s_d(x)$ and the free-stream speed U. For the wing-body combination, this similarity no longer applies, since the body radius r provides a further length-scale.

To make a comparison with the results for the wing alone, the present method should be applied for a vanishingly small value of r. In terms of the

non-dimensional variables introduced in section 4, this means an indefinitely large value of s (the semi-span divided by r) and a vanishingly small value of P ($= -\Omega r/U$), such that the product Ps remains finite and equal to $-\Omega s_d/U$. In practice, we are limited to finite values of s and P, so calculations have been made for Ps equal to the values of $-\Omega s_d/U$ appropriate to the measurements, for several small values of P. It is apparent from these that the solutions depend little on P, unless Ps is small, and some features of the solutions can be extrapolated to $P = 0$ with confidence.

The values of P chosen are 0.04, 0.02 and 0.01. The semi-apex angle of Harvey's wing is 10°. As explained in the previous section, the downstream integration starts with an initial solution appropriate to a delta wing at an angle of incidence, α, equal to P. The values of the incidence parameter $\alpha/\tan\gamma$ corresponding to these three rates of roll are therefore 0.227, 0.113 and 0.057. The last two of these are below the range for which solutions could be found by Smith[4], using a polar representation of the sheet, but Barsby[5] obtained solutions using the same intrinsic coordinate system as the present treatment. At the lowest value of $\alpha/\tan\gamma$ the sheet has a marked inflexion, and at only slightly lower values Barsby found that he could only obtain solutions by allowing the separation point to move inboard from the leading edge. We note in passing that the present results cannot be generalized to other values of γ, in the way that the results of Hanin and Mishne[22], using an isolated vortex model for the rolling delta wing, can be generalized.

The number, n, of points representing the sheet was chosen to be 12. A similar degree of detail was found adequate by Smith[4] and the need to carry the calculations to large values of s in reasonable time argued against an unnecessarily large value.

The marching procedure in all these cases was started in the cross-flow plane for which $s = 1.1$, that is $x = x_0 = 0.1/\gamma$ and the quantity ℓ used in the definition of η, (58), was specified as

$$\ell = (s - 1) + 0.01(x - x_0)^2 \quad . \tag{68}$$

In the immediate neighbourhood of the initial station, ℓ grows like $(x - 1)$ as required for a conical approximation, and increases quadratically as we march further downstream.

In his experimental investigations Harvey obtained detailed pressure measurements on the wing surface at three locations on the wing, namely $x/c = 0.333$, 0.556 and 0.778, where c is the root chord of the wing, and at the three different roll rates

$$-\frac{\Omega s_d(c)}{U} = 0.1,\ 0.2 \text{ and } 0.3 .$$

Thus we have results for nine values of Ps available from the experiments namely 0.0333, 0.0556, 0.0666, 0.0778, 0.0999, 0.1112, 0.1556, 0.1668 and 0.2334. These are the values for which a detailed analysis of the results obtained has been carried out.

6.2 Vortex sheet shapes and circulations

In Fig 4 we show the vortex sheet shape and vortex position, scaled with the local semi-span s , for P = 0.01 at various streamwise stations. These streamwise stations correspond with the values taken by Ps in Harvey's experiments. The vortex system grows downstream in a non-conical fashion, as can be seen, but the form specified for $\ell(x)$ in (68) ensures that the angular extent of the sheet remains almost constant. This appears to be a happy coincidence, for although the quadratic behaviour of $\ell(x)$ may reflect some underlying structure to the solutions we have been unable to expose it. This constant angular extent is also maintained in the results for P = 0.02 and 0.04 , and in Fig 5 the sheet shapes for the three rates of roll are shown for certain of the values of Ps . These demonstrate that the different body size has little influence upon the sheet shapes once the semi-span is large compared to the body diameter, and in particular, that P = 0.01 is small enough for the effects of the body on the sheet shape to be small for these values of Ps . The positions of the isolated vortices are again shown in Fig 6 and are seen to remain close together for the different values of P . Thus the vortex position does not depend significantly on r/s . Harvey measured the total head distribution in the planes x/c = 0.5, 0.6 and 0.7 for the same angular velocities as in his pressure measurements. The smallest of the contours of total head surrounding the vortex cores which he was able to draw are also shown in Fig 6, for the highest angular velocity. These show that vortex cores in the experiment were slightly lower than the isolated vortices in the calculation and about 5% of the semi-span further inboard. This discrepancy is about the same as that found in the case of a delta wing at incidence, which is provisionally ascribed to the effects of secondary separation in Ref 4.

Hanin and Mishne[22] have carried out a calculation for the separated flow past a rolling delta wing using an isolated vortex model, following Brown and Michael[2]. The resulting vortex positions are also shown in Fig 6. As for the case of a fixed delta wing at incidence the predicted height of the vortex agrees

well with that given by the vortex sheet model while the lateral distance of the vortex from the wing centre line is significantly overestimated.

The total circulation (non-dimensional) on the vortex sheet and isolated vortex, divided by Ps^2, is plotted in Fig 7. In dimensional variables this corresponds to the total circulation divided by $-\Omega s^2$. The graph shows this quantity rising fairly quickly, as Ps increases, to a plateau of roughly constant height, showing that the circulation is about $1.5\ Ps^2$ for $s > 5$. Hanin and Mishne[22] found that the first term in the expansion (for small rate of roll) for the circulation of the isolated vortex is proportional to $-\Omega s^2$, but it is not clear how significant this correspondence is.

6.3 Wing surface pressures

From Bernoulli's equation (14) and relation (19) the pressure coefficient is given by

$$C_p = -2\Phi_x - \left(\Phi_y^2 + \Phi_z^2\right) + 2P\left\{\Phi_y z - \Phi_z y\right\} .$$

The velocity components Φ_y and Φ_z may be calculated directly from the real and imaginary parts of $\partial W/\partial Z$ but Φ_x must be evaluated using a difference formula for the downstream derivative. In order, therefore, to determine the pressure coefficient at a point $(x_m + h_x/2,\ y,\ 0)$ on the wing we evaluate the vector $\underline{X}(x_m + h_x/2)$ from $\underline{X}(x_m)$ and $\underline{X}(x_m + h_x)$ by linear interpolation as in (57) and hence determine Φ_y and Φ_z. To determine the downstream derivative of the potential, Φ_x, in the cross-flow plane $x_m + h_x/2$, we calculate the potential $\Phi = R\{W\}$ for the same value of y in the planes $x = x_m$ $x = x_m + h_x$ using the result obtained by integrating (54), namely

$$W(\zeta) = W_A(\zeta) + \frac{\Gamma}{2\pi i}\left\{\log\left(\frac{\zeta - \zeta_v}{\zeta - \frac{1}{\bar{\zeta}_v}}\right) + \log\left(\frac{\zeta + \zeta_v}{\zeta + \frac{1}{\bar{\zeta}_v}}\right)\right\}$$

$$+ \int_0^{\tau_E} -\frac{1}{2\pi i}\frac{\partial \Lambda\Phi}{\partial \sigma}\frac{\partial \sigma}{\partial \tau}\left\{\log\left(\frac{\zeta - \zeta(\tau)}{\zeta - \frac{1}{\bar{\zeta}(\tau)}}\right) + \log\left(\frac{\zeta + \zeta(\tau)}{\zeta + \frac{1}{\bar{\zeta}(\tau)}}\right)\right\} d\tau . \quad (69)$$

The constant of integration in (69), which could in principle depend on x, has been chosen to be zero, so as to ensure that Φ_x, and therefore C_p, tends to zero at infinity.

We then calculate ϕ_x using the central difference formula (56). When evaluating (69) care must be taken to ensure that the correct branch of the complex logarithm is taken. This is determined by the criterion that the logarithm is continuous everywhere except across the vortex sheet where it jumps discontinuously by $2\pi i$. The numerical techniques used to evaluate the integral in (69) are similar to those described in section 5.

Detailed pressure distributions over the wing surface for $P = 0.04$, 0.02 and 0.01 are shown in Figs 8 to 13, in which the pressure coefficient is plotted against the distance from the centre line, non-dimensionalised with respect to the overall semi-span. The pressure coefficient was not calculated over the body as it makes no contribution to the rolling moment, and so an indication of the relative size of the body and wing is given by the ordinate at which each pressure distribution terminates. Each figure is for a particular value of Ps and so the smaller body sizes correspond to the smaller values of P . For the lower values of Ps the suction peaks on the upper surface are very high and narrow; as Ps increases the height of these peaks falls slightly, but they broaden considerably. These peaks also illustrate that the solutions for different values of P but the same value of Ps are very close. For the higher values of Ps the experimentally measured pressure coefficients of Harvey[21] are superposed. In most of these cases the agreement is good only away from the suction peak and, as for the case of a wing at incidence, in the region of the peak the experimental curves are lower and broader. For the last case, however, $Ps = 0.2334$, the agreement is very good. The pressure distributions calculated by Hanin and Mishne[22] are not shown as their calculated suction peaks are considerably higher and narrower than those shown here.

Several factors may be responsible for the differences between the calculated and measured pressure distributions. It could be that the presence of the body is affecting the calculated values. This effect would be largest for the smallest value of Ps , yet Fig 9 shows that the effects of a four-fold change in body size are negligible compared with the difference between the calculated and measured pressures at $Ps = 0.08$. At the streamwise station nearest to the trailing edge, $x/c = 0.778$, the upstream influence of the trailing edge, neglected in the theory, could be expected to affect the measured values. Results for this station are shown in Figs 9, 11 and 13, and it is difficult to identify any consistent discrepancy in these three figures. It appears therefore that upstream influence of the trailing edge is fairly small on this wing at this station, which is about 1.25 semi-spans ahead of the trailing edge.

The flow on the upper surface underneath the vortex is directed outboard relative to the vortex and encounters a rising pressure between the vortex and the leading edge. This pressure rise will tend to produce a secondary separation of the boundary layer, not represented in the theoretical model. Certainly the very steep gradients and large pressure rises predicted by the theory for the smaller values of Ps seem incompatible with attached boundary layers, either laminar or turbulent. On the other hand, Harvey suggests that no secondary separation occurred in his experiments, on the grounds that appreciable pressure rises were observed between the vortex and the leading edge. He attributes the absence of separation to a thinning of the boundary layer, produced by the rotation of the wing. At the time of Harvey's work, almost all the available pressure distributions on wings with leading-edge vortices had been measured in circumstances in which the boundary layer was laminar at secondary separation, and in these circumstances little pressure rise is observed. Since then, appreciable recompression of the flow outboard of the vortex has been found on wings at incidence, in cases where the boundary layer is turbulent in this region, see for example Ref 30. Typically, the turbulent boundary layer sustains a larger pressure rise before separating, and then separates further outboard, than the laminar layer. Comparison with typical shapes of measured suction peaks[30] suggests that those in Figs 11 and 13 and, probably Fig 9 are associated with turbulent secondary separation and that those in Fig 10 and, possibly, Fig 12 correspond to laminar secondary separation. This would imply that transition occurred between $x/c = 0.556$ and 0.778, *ie* at a Reynolds number of between 5 and 7×10^5 based on distance from the apex. This is somewhat lower than the corresponding Reynolds number for wings of aspect ratio 1 at moderate incidence[30]. In the absence of direct observations, it is thought likely therefore that secondary separation was present in Harvey's experiments. In the more thoroughly examined flow over a wing at incidence, it has been argued[4] that the discrepancy between the calculated and measured suction peak is due to secondary separation, largely on the basis that transition has a marked effect on the form of the suction peak. We therefore ascribe most of the difference between the calculated and measured suction peaks to the absence of a representation of secondary separation in the theoretical model.

6.4 The local rolling moment

The quantity of most practical interest is the rolling moment induced by the rolling motion, the damping in roll. The present approach lends itself most readily to the calculation of the local rolling moment, *ie* the rolling moment acting on a narrow element of the wing between two neighbouring cross-flow planes,

divided by the distance between them. This is also the quantity derived by Harvey[21] from his pressure measurements. The local rolling moment can be expressed conveniently in coefficient form by referring it to the product of the kinetic pressure ($\frac{1}{2}\rho U^2$) and the square of the local span. This coefficient is divided by the roll rate parameter, $-\Omega s/U$, to give a quantity which varies slowly with roll rate, and would be the constant stability derivative in a linear model of the flow. Thus we have a derivative, $C_{\ell p}$, of the local rolling moment coefficient given by

$$C_{\ell p} = \frac{\text{rolling moment/unit chord}}{\frac{1}{2}\rho U^2 4s^2 \left(-\frac{\Omega s}{U}\right)} ,$$

where the quantities are dimensional. Hence

$$C_{\ell p} = \frac{1}{2Ps} \int_0^1 \Delta C_p(x, y) \frac{y}{s} \, d\left(\frac{y}{s}\right)$$

where the quantities are now non-dimensional.

For the case of a rolling slender delta wing in attached flow this may easily be evaluated (cf. Harvey[21]) to give

$$C_{\ell p} = -\frac{\pi}{4} \tan \gamma .$$

The attached-flow rolling moment for the wing-body combination was evaluated numerically, using a subroutine QA04A, from the Harwell Subroutine Library, which automatically takes care of the square root singularity at the leading edge. These results agree very closely with the formula

$$C_{\ell p} = -\frac{\tan \gamma}{\pi} \frac{(s^4 - 1)}{s^4} \left\{ \frac{s^2 + 1}{s^2} \tan^{-1} s + \frac{s^2 - 1}{s(s^2 + 1)} \right\}^{\frac{1}{2}} , \qquad (70)$$

which is derived by differentiating the overall rolling moment coefficient calculated by Lomax and Heaslet[23]. This coefficient is sketched against Ps in Fig 14 for attached flow and for $P = 0.01$. For the rolling wing-body combination the coefficient quickly rises from zero, overshoots the value for the delta wing and then settles down very close to this line.

Simple flow models, the isolated vortex model (Hanin and Mishne[22]) and the leading-edge suction analogy model (see the Appendix) may also be employed to give values for the local rolling moment coefficient for the delta wing. These are also sketched in Fig 14. To determine the effect of the body upon the solutions, calculations were carried out using the isolated vortex model applied to a rolling wing-body combination. In these calculations the numerical method discussed earlier in section 5 was employed, except that no vortex sheets were present and therefore only the Kutta condition and zero force condition were used. These results, for $P = 0.01$ and 0.02 are shown in Fig 14. Comparing the results with those of Hanin and Mishne[22] for $P = 0$ we see that at the larger values of Ps both sets of solutions, with and without the body, are in close agreement although they differ considerably for the lower values of Ps. To attempt to eliminate the effect of the body we may linearly extrapolate the results of the isolated vortex model for $P = 0.02$ and 0.01 to $P = 0$, corresponding to $r = 0$, the rolling delta wing. In this way we do indeed reproduce the results of Hanin and Mishne, except for $Ps = 0.033$ where the effect of the body is significant. This may be easily seen in Fig 14, since, for $Ps > 0.04$, the difference between the curves for $P = 0.02$ and 0.01 is equal to the difference of the results for $P = 0.01$ and those of Hanin and Mishne for $P = 0$. We should therefore expect a reasonable approximation for a rolling delta wing to be given by extrapolating the calculated results to $P = 0$. Similarly an analysis may also be carried out using the leading-edge suction analogy and the results are sketched in Fig 14. The details of the method are given in the Appendix. Those again show that extrapolation of the curves for $P = 0.02$ and 0.01 to $P = 0$ reproduce the results for the case when no body is present. For the full vortex sheet model, therefore, we should expect a reasonable approximation for a rolling delta wing to be given by extrapolating the results for low values of P to $P = 0$.

This local rolling moment coefficient was evaluated for the full vortex sheet model for a range of values of Ps, with $P = 0.01$, 0.02 and 0.04. The integration technique used employed Simpson's rule over 100 and 200 integration points, together with Richardson extrapolation to increase the accuracy. As a check upon the accuracy some of the integrations were repeated using 200 and 400 integration points with no appreciable difference in the results. The rolling moment coefficients are shown in Fig 15. For fixed Ps the suction peaks are always slightly higher for the larger values of P. Also, since they are close to the leading edge the fact that they are higher has a significant effect on the rolling moment. This effect far outweighs the extra contributions from the larger wing length for the smaller values of P, corresponding to the smaller body sizes.

Consequently the rolling moment coefficients are in general larger for large P, except in those cases for which the wing span is not much bigger than the body diameter.

As we mentioned earlier, we should expect a reasonable approximation for a rolling delta wing to be given by extrapolating the results for the wing-body combination to $P = 0$. This extrapolated curve is indicated in Fig 15.

In Fig 16 the experimental results of Harvey are given, together with the extrapolated results for $P = 0$ from the different theories. We see that the isolated vortex model considerably overpredicts the magnitude of the local rolling moment coefficient. This is because the calculated suction peaks are too far outboard and too high. The leading-edge suction analogy, however, gives better agreement. As can be expected from the pressure distribution shown in Figs 8 to 13, the results for the vortex sheet model agree well with the experimental value for $Ps = 0.2334$ but not so well for smaller values of Ps. Any difference between the theoretical and experimental pressure distributions close to the leading edge of the wing will of course be magnified when calculating the rolling moment. When secondary separation is present the modification to the pressure distribution in flows of this type is such that the normal force is, in general, predicted correctly. When this is the case the rolling moment cannot be predicted correctly. It is not surprising therefore that the closest agreement between theory and experiment occurs for the experimental results associated with the station closest to the trailing edge and the highest rate of roll. For, in spite of the upstream effect of the trailing edge in this case, the fact that the separation is turbulent in the experiments leads to a pressure distribution similar to that predicted by the theoretical calculations.

7 CONCLUSIONS

The vortex sheet model of leading-edge separation has been successfully adapted to calculate the positions and strengths of the leading-edge vortices, the pressure distribution over the wing and the local rolling moment of slender delta wings mounted on cylindrical bodies in steady rolling motion at zero incidence.

Comparisons with the experimental observations of Harvey suggest that the model describes this flow as well as it describes the flow past a slender wing at incidence. However, because the discrepancies occur close to the leading edge, the prediction of rolling moment due to roll is less accurate than the prediction of lift due to incidence. The vortices in both flows are found to lie inboard of their calculated positions to 3 to 5% of the local semi-span; and the form of the

measured pressure distribution agrees best with the calculation when the Reynolds number is higher and the boundary layer can be assumed turbulent at secondary separation. These are also the conditions in which the prediction of the rolling moment is most accurate.

The results confirm the measurements and the predictions of simpler models[22,31] that leading-edge separation increases the roll damping. The present predictions are more realistic than those of the isolated vortex model. They also show that the presence of the body (in a configuration of fixed total span) increases the roll damping unless the exposed wing span is very small.

Acknowledgments

The author would like to thank Dr J.E. Barsby of ICL Ltd, Professor N. Riley of the University of East Anglia and Mr J.H.B. Smith of the Royal Aircraft Establishment for their help and guidance throughout the period of research.

Appendix

APPLICATION OF THE LEADING-EDGE SUCTION ANALOGY

The results presented earlier for the rolling moment coefficient have also been compared with some results obtained using an empirical method derived by Polhamus[19] for calculating the lift on a slender wing and later extended to the rolling case by Boyden[31]. In this theory the nonlinear lift force acting on the wing is represented by the force arising from the singularity at the leading edge of the wing. In his paper Boyden used lifting surface theory to obtain the linear and nonlinear lift contributions but in the present work we just use the results predicted by slender body theory, for consistency with the other models used.

From Robinson and Laurmann[32] the leading-edge suction force per unit chord is given by

$$\underline{F} = \text{real}(-\pi\rho C^2) \tag{A-1}$$

where C is defined by

$$\frac{\partial W_A}{\partial Z} = f(Z - s) + \frac{C}{\sqrt{Z - s}}$$

in the neighbourhood of the leading edge, $Z = s$. In the present case, from (4) we have, in dimensional notation

$$\frac{\partial \zeta}{\partial Z} = \sqrt{\frac{s^2 - r^2}{2s(s^2 + r^2)}}\,\frac{1}{\sqrt{Z - s}} + O(1)$$

and hence

$$\frac{\partial W_A}{\partial Z} = \frac{\partial W_A}{\partial \zeta}(\zeta = 1)\sqrt{\frac{s^2 - r^2}{2s(s^2 + r^2)}}\,\frac{1}{\sqrt{Z - s}} + O(1)$$

where $\partial W_A/\partial \zeta$ is given by (13). Hence

$$C = \frac{\partial W_A}{\partial \zeta}(\zeta = 1)\sqrt{\frac{s^2 - r^2}{2s(s^2 + r^2)}} \tag{A-2}$$

and so, through (A-1) the suction force $\underline{F}$ acting on the leading edge may be calculated. This force acts in a direction tangential to the wing surface and, according to Polhamus, the nonlinear force acting on the wing due to the leading-edge separation is given by rotating the force $\underline{F}$ through 90^{o} so that it acts perpendicular to the wing. Assuming that this force still acts through the leading edge the magnitude of the local moment per unit chord is given by $s|\underline{F}|$. Now

$$C_{\ell p} = \frac{\text{rolling moment/unit chord}}{\frac{1}{2}\rho U^2 4s^2 \left(-\frac{\Omega s}{U}\right)}$$

where the quantities are dimensional. Hence from (A-1) we obtain the rolling moment coefficient due to the suction on both sides of the wing

$$(C_{\ell p})_{\text{nonlinear}} = -\pi \frac{|\mathrm{Re}(C^2)|}{Ps^2} \tag{A-3}$$

where the quantities are now non-dimensional. C is given from (A-2) as

$$C = \frac{\partial W_A}{\partial \zeta}(\zeta = 1)\sqrt{\frac{s^2 - 1}{2s(s^2 + 1)}} \tag{A-4}$$

and so, through (A-1) the force $\underline{F}$ acting on the singularity may be calculated.

The total rolling moment coefficient is then found by adding on the contribution from the attached flow potential. Now, at the leading edge, from (13), we have

$$\left.\frac{\partial W_A}{\partial \zeta}\right|_{\zeta=1} = \frac{-iP}{\pi \cos^2\theta_1}(\pi + 2\theta_1 + \sin 2\theta_1) \tag{A-5}$$

where $\cos\theta_1 = 2s/(1 + s^2)$. Since

$$\theta_1 = \cos^{-1}\frac{2s}{1 + s^2} = 2\tan^{-1}s - \frac{\pi}{2},$$

we obtain from (A-3), (A-4) and (A-5)

Appendix A

$$(C_{\ell p})_{\text{nonlinear}} = -\frac{P(s^4 - 1)}{2\pi s^3}\left\{\frac{s^2 + 1}{s^2}\tan^{-1}s + \frac{s^2 - 1}{s(s^2 + 1)}\right\}^2 .$$

Hence, from (70)

$$C_{\ell p} = (C_{\ell p})_{\text{attached}} + (C_{\ell p})_{\text{nonlinear}}$$

$$= -\frac{(s^4 - 1)}{\pi s^4}\left(\tan\gamma + \frac{Ps}{2}\right)\left\{\frac{s^2 + 1}{s^2}\tan^{-1}s + \frac{s^2 - 1}{s(s^2 + 1)}\right\}^2 .$$

This is sketched in Fig 14 for $P = 0.0$, 0.01, 0.02 and 0.04 .

LIST OF SYMBOLS

$\underline{a}$, $\underline{b}$	unit vectors in tangent plane to the vortex sheet
C	constant (see Appendix)
$C_{\ell p}$	local rolling moment coefficient
$\underline{F}$	vector of residuals
g	$= - \partial\Delta\Phi/\partial\tau\|_{\eta}$
h_x	downstream step length
h_τ	step length in cross-flow plane
i	$\sqrt{-1}$
$\underline{i}$, $\underline{j}$, $\underline{k}$	unit vectors
ℓ	function of x used to maintain a constant angular extent for the sheet
n	number of intermediate points on the sheet
$\underline{n}$	unit outward normal to the wing-body combination and vortex sheet
p	pressure
P	roll rate parameter ($= - \Omega r/U$)
$\underline{q}$	velocity vector relative to the wing-body combination
q_t	relative velocity tangential to the sheet in the cross-flow plane
q_n	relative velocity normal to the sheet in the cross-flow plane
r	radius of body
s	wing-body semi-span
t	time
$\underline{u}$	velocity vector
W	complex potential
W_A	attached flow complex potential
$\underline{X}$	vector of unknowns for Newton iteration
(x, y, z)	Cartesian coordinates
Z	$= y + iz$
Z_V	position of isolated vortex in cross-flow plane
γ	wing semi-apex-angle
Δ	difference operator across the vortex sheet
η	coordinate on the vortex sheet
ζ	coordinate in complex transformed cross-flow plane
ζ_V	position of isolated vortex in the transformed plane
θ_1	$= \cos^{-1}\left(2rs/(r^2 + s^2)\right)$
λ, μ	scalar quantities (section 3)
(ξ, η, ψ)	coordinate system (section 3)
ρ	density

LIST OF SYMBOLS (concluded)

σ	arc length
Σ	vortex sheet (section 3)
τ	stretched coordinate on sheet
Φ	velocity potential
ψ	angle between tangent to sheet and wing

The same symbols have been used for dimensional quantities before section 4.3 and for quantities non-dimensionalized using r and U later in the main text. In the Appendix both dimensional and non-dimensional quantities are used.

REFERENCES

No.	Author	Title, etc
1	R. Legendre	Écoulement au voisinage de la pointe avant d'une aile à forte fléche aux incidences moyennes. 8th Int. Cong. Th. Appl. Mech. Istanbul (1952); also Rech. Aéro. No. 30 (1952) and Rech. Aéro. No. 31 (1953)
2	C.E. Brown W.H. Michael	On slender delta wings with leading-edge separation. *J. Aero. Sci.*, pp 690 and 706 (1954); also NACA TN 3430 (1955)
3	K.W. Mangler J.H.B. Smith	A theory of the flow past a slender delta wing with leading-edge separation. RAE Report Aero 2593 (1957); also *Proc. Roy. Soc.*, A 251, p 200 (1959)
4	J.H.B. Smith	Improved calculations of leading-edge separation from slender delta wings. RAE Technical Report 66070 (1966)
5	J.E. Barsby	Separated flow past a slender delta wing at incidence. *Aero. Quart.*, 24, pp 120-128 (1973)
6	J.H.B. Smith	Calculations of the flow over thick, conical slender wings with leading-edge separation. RAE Technical Report 71057 (1971); ARC R & M No.3694 (1972)
7	J.E. Barsby	Calculations of the effect of blowing from the leading edges of a slender delta wing. RAE Technical Report 71077 (1971); ARC R & M No.3692 (1972)
8	J.E. Barsby	Flow past conically-cambered slender delta wings with leading-edge separation. RAE Technical Report 72179 (1972)
9	D.I. Pullin	Calculations of the steady conical flow past a yawed slender delta wing with leading-edge separation. Imperial College Aero Report 72-17 (1972)
10	I.P. Jones	Flow separation from yawed delta wings. *Computers and Fluids*, 3, pp 155-177 (1975)

REFERENCES (continued)

No.	Author	Title, etc
11	E.S. Levinsky M.H.Y. Wei	Nonlinear lift and pressure distribution on slender conical bodies with strakes at low speeds. NASA CR-1202 (1968)
12	J.H.B. Smith	A theory of the separated flow from the curved leading edge of a slender wing. ARC R & M No.3116 (1957)
13	D.G. Randall	A theoretical determination of the flow past and the air forces on an oscillating slender delta wing with leading-edge separation. RAE Report Structures 284 (1963)
14	J.H.B. Smith	Boundary conditions on a vortex sheet. RAE Technical Memorandum Aero 1368 (1971)
15	J.H.B. Smith	Similar solutions for slender wings with leading-edge separation. *Presented at 13th Int. Cong. of Theoretical and Applied Mechanics (1972)*
16	R.W. Clark	Non-conical flow past slender wings with leading-edge vortex sheets. RAE Technical Report 76037; ARC R & M No.3814 (1976)
17	I.P. Jones	Leading-edge separation from non-conical slender wings at incidence. Proc. 4th Int. Conf. on Numerical Methods in Fluid Dynamics (1974); *Lecture notes in Physics*, 35, pp 225-321, Springer (1975)
18	A.H. Sacks R.E. Lundberg C.W. Hanson	A theoretical investigation of the aerodynamics of slender wing-body combinations exhibiting leading-edge separation. NASA CR-719 (1967)
19	E.C. Polhamus	A concept of the vortex lift of a sharp edge delta wing based on a leading-edge suction analogy. NASA TN D-3767 (1966)

REFERENCES (continued)

No.	Author	Title, etc
20	G.N. Ward	*Linearised theory of steady high-speed flow.* Cambridge University Press (1955)
21	J.K. Harvey	An investigation into the flow past a slender delta wing which is rolling at zero incidence in an airstream. Imperial College Aero Report 105 (1960); also *J. Roy. Aero. Soc.*, 68, pp 106-110 (1964)
22	M. Hanin D. Mishne	Flow about a rolling slender wing with leading-edge separation. *Israel J. of Technology*, 11, No.3, p 131-136 (1973)
23	H. Lomax M. Heaslet	Damping-in-roll calculations for slender swept-back wings and slender wing-body combinations. NACA TN 1950 (1949)
24	G.J. Adams D.W. Dugan	Theoretical damping in roll and rolling moment due to differential wing incidence for slender cruciform wings and wing-body combinations. NACA TN 1088 (1952)
25	P.J. Bobbitt F.S. Malvestuto	Theoretical damping in roll and rolling moment due to differential wing incidence for slender cruciform wings and wing-body combinations. NACA TN 1088 (1952)
26	I.P. Jones	Leading-edge vortex flows. PhD Thesis, University of East Anglia (1974)
27	H.P. Greenspan	*The theory of rotating fluids*, p 6. Cambridge University Press (1968)
28	J.E. Barsby	Calculations of the effect of blowing from the leading edges of a cambered delta wing. ARC R & M No.3800 (1978)
29	G. Forsythe C.B. Moler	*Computer solution of linear algebraic systems.* Prentice Hall (1967)
30	J.H.B. Smith A.G. Kurn	Pressure measurements on a slender rhombic cone at incidence, at Mach numbers from 0.4 to 1.1. RAE Technical Report 68171 (1968); ARC R & M No.3626 (1968)

REFERENCES (concluded)

No.	Author	Title, etc
31	R.P. Boyden	Effects of leading-edge vortex flow on the roll damping of slender wings. *J. Aircraft*, 8, No.7, p 543 (1971)
32	A. Robinson J.A. Laurmann	*Wing theory.* Cambridge University Press (1956)

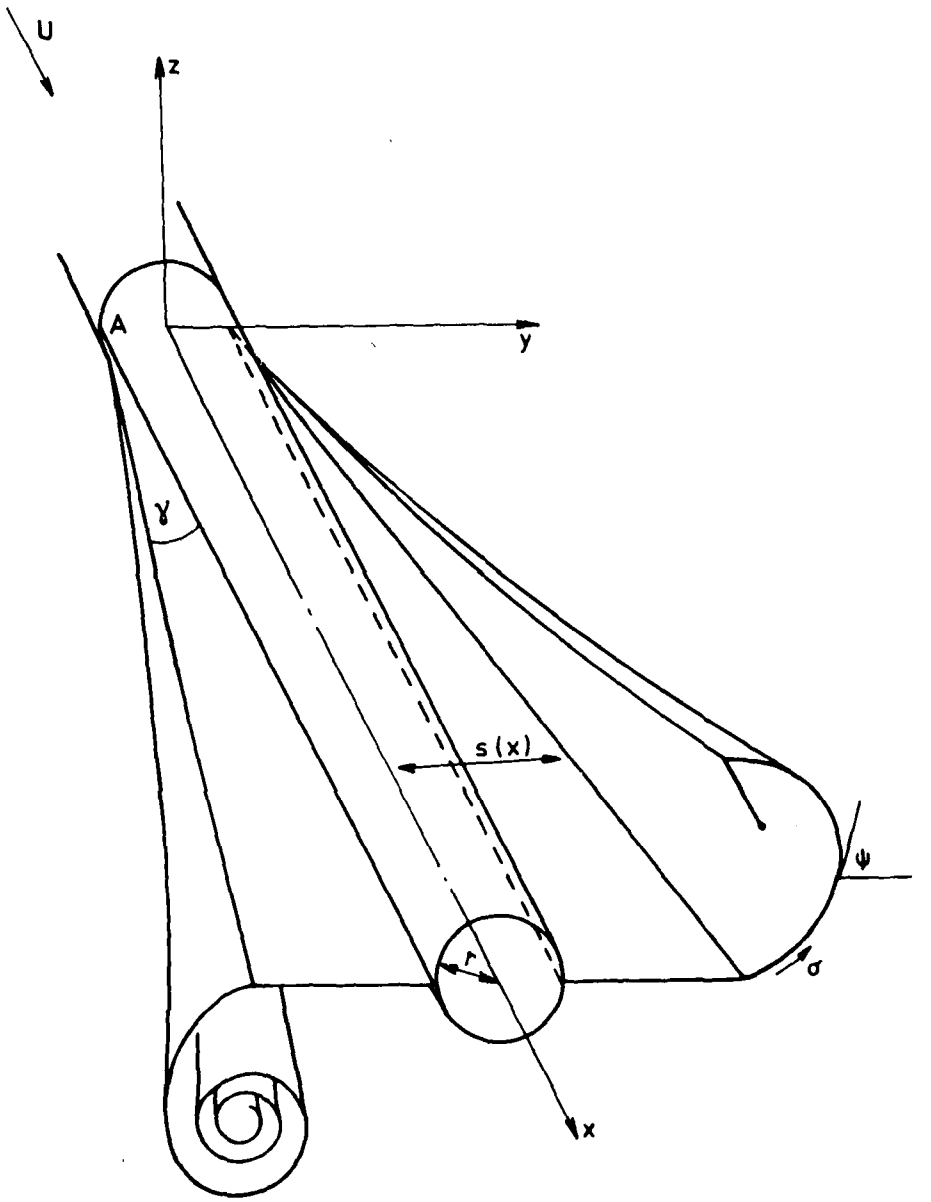

Fig 1 The rolling wing-body combination

Fig 2a&b

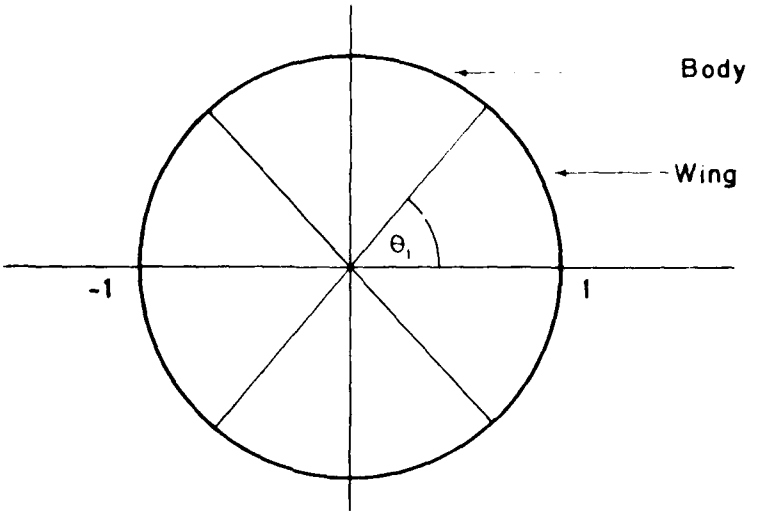

Fig 2a The transformed plane

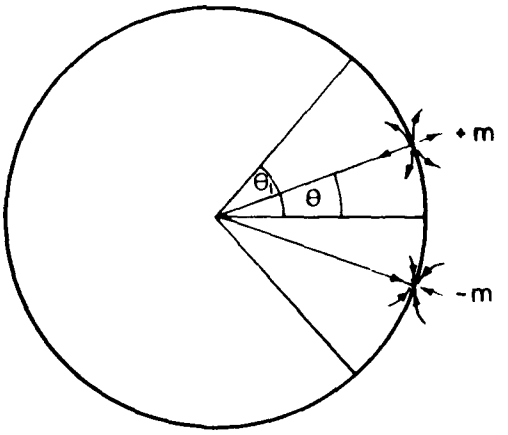

Fig 2b Source-sink distribution

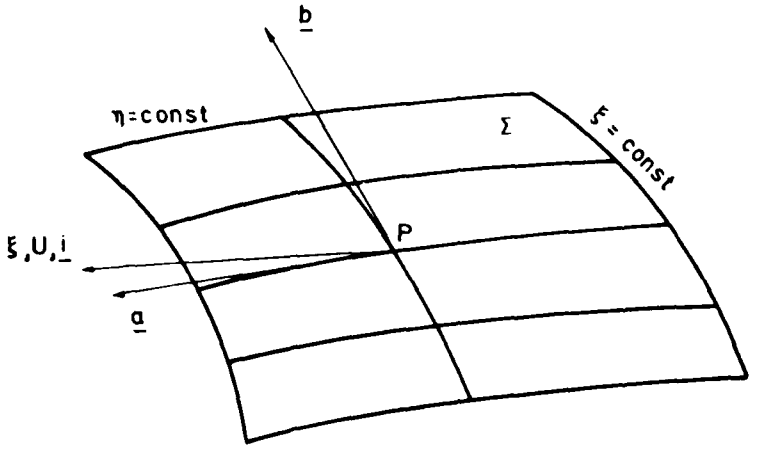

Fig 3a The vortex sheet Σ

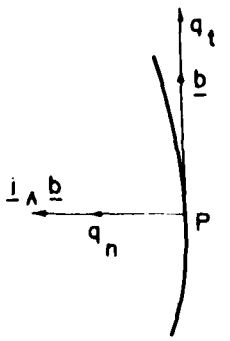

Fig 3b The cross-flow plane

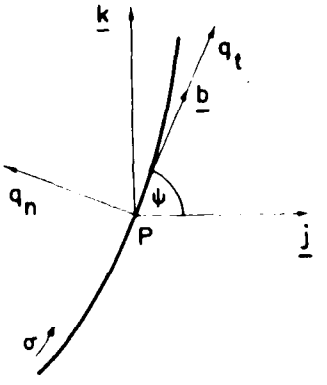

Fig 3c Intrinsic coordinates

Fig 4

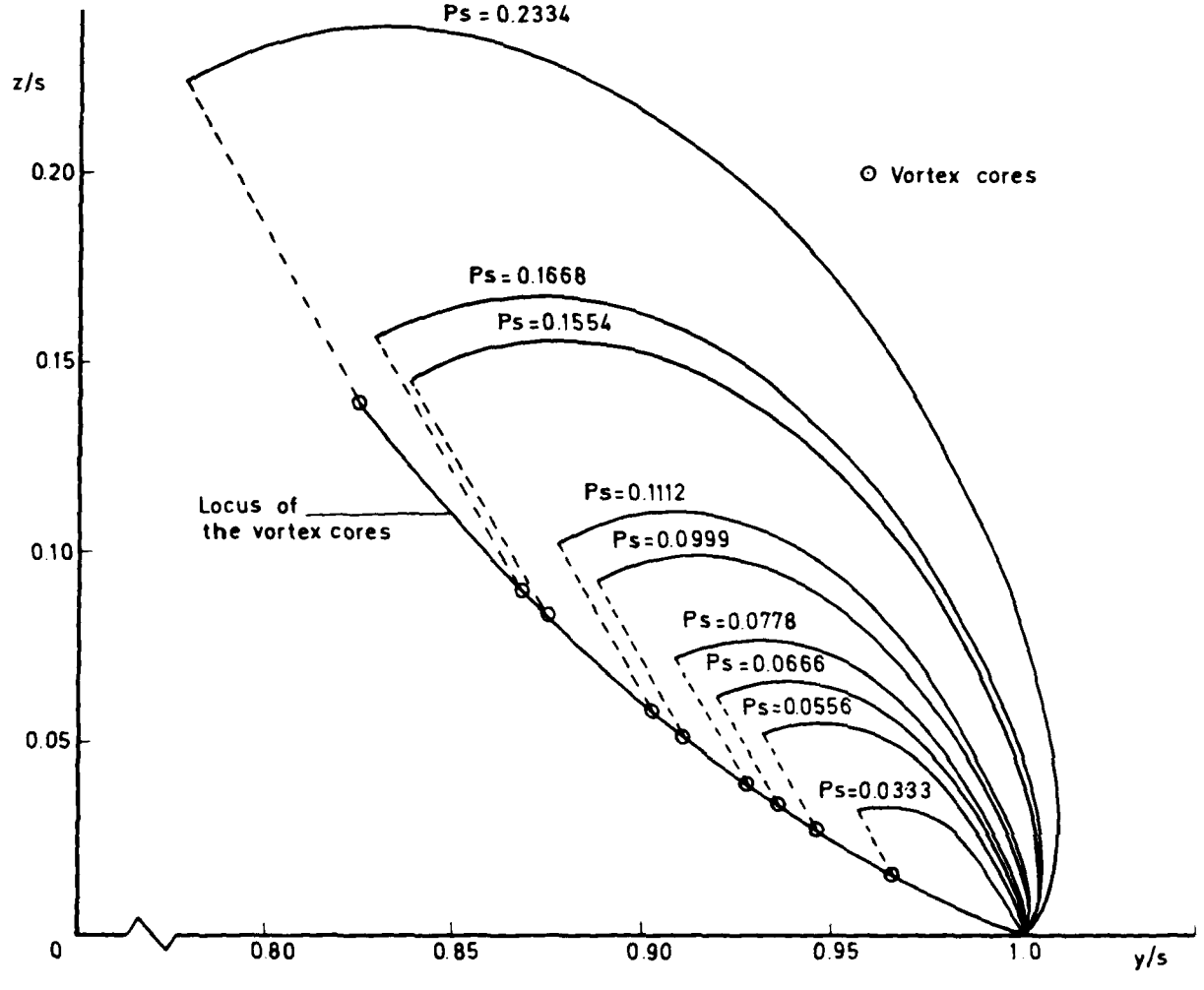

Fig 4 Vortex sheet shapes, P = 0.01

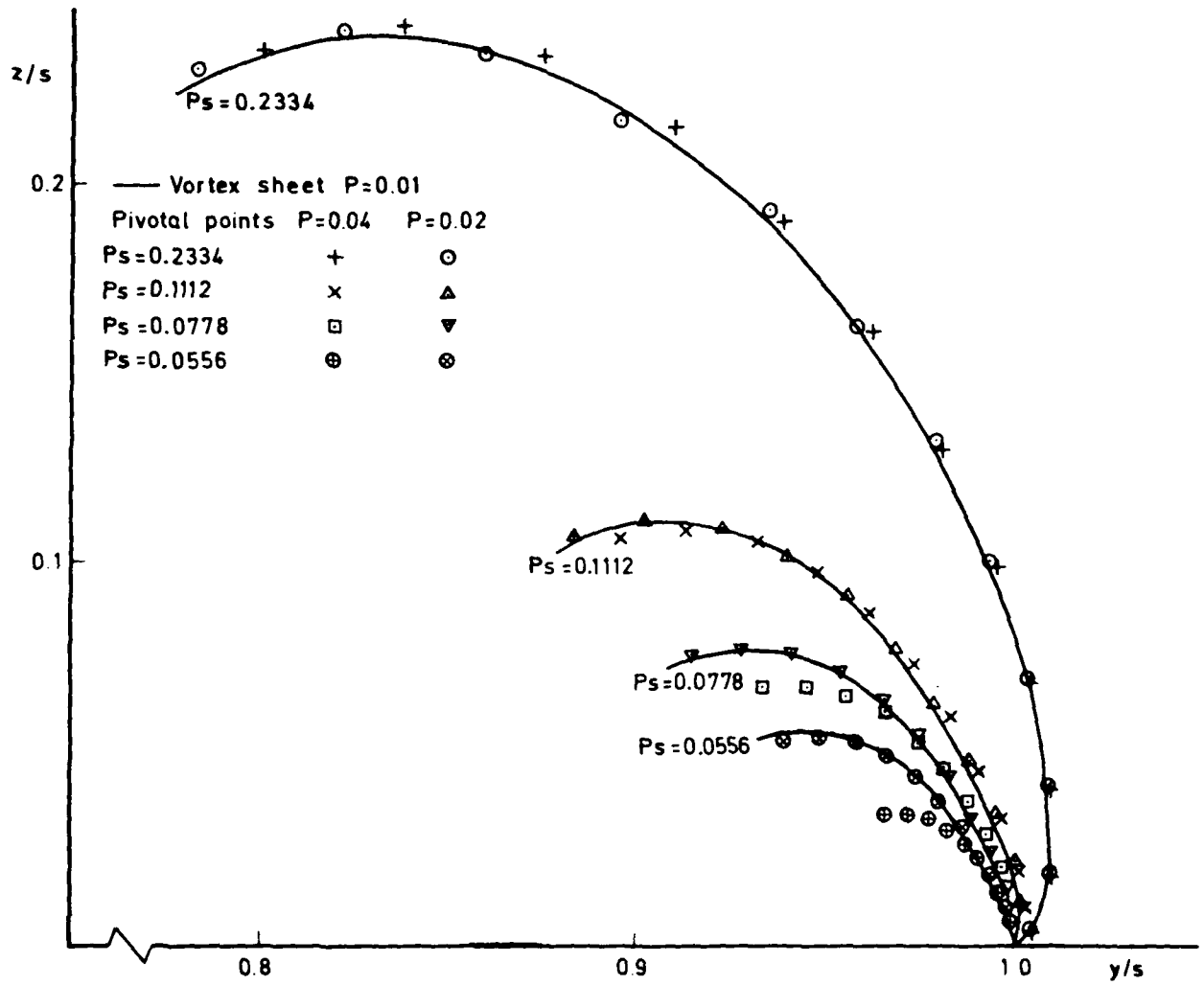

Fig 5 Comparison of vortex sheet shapes

Fig 6

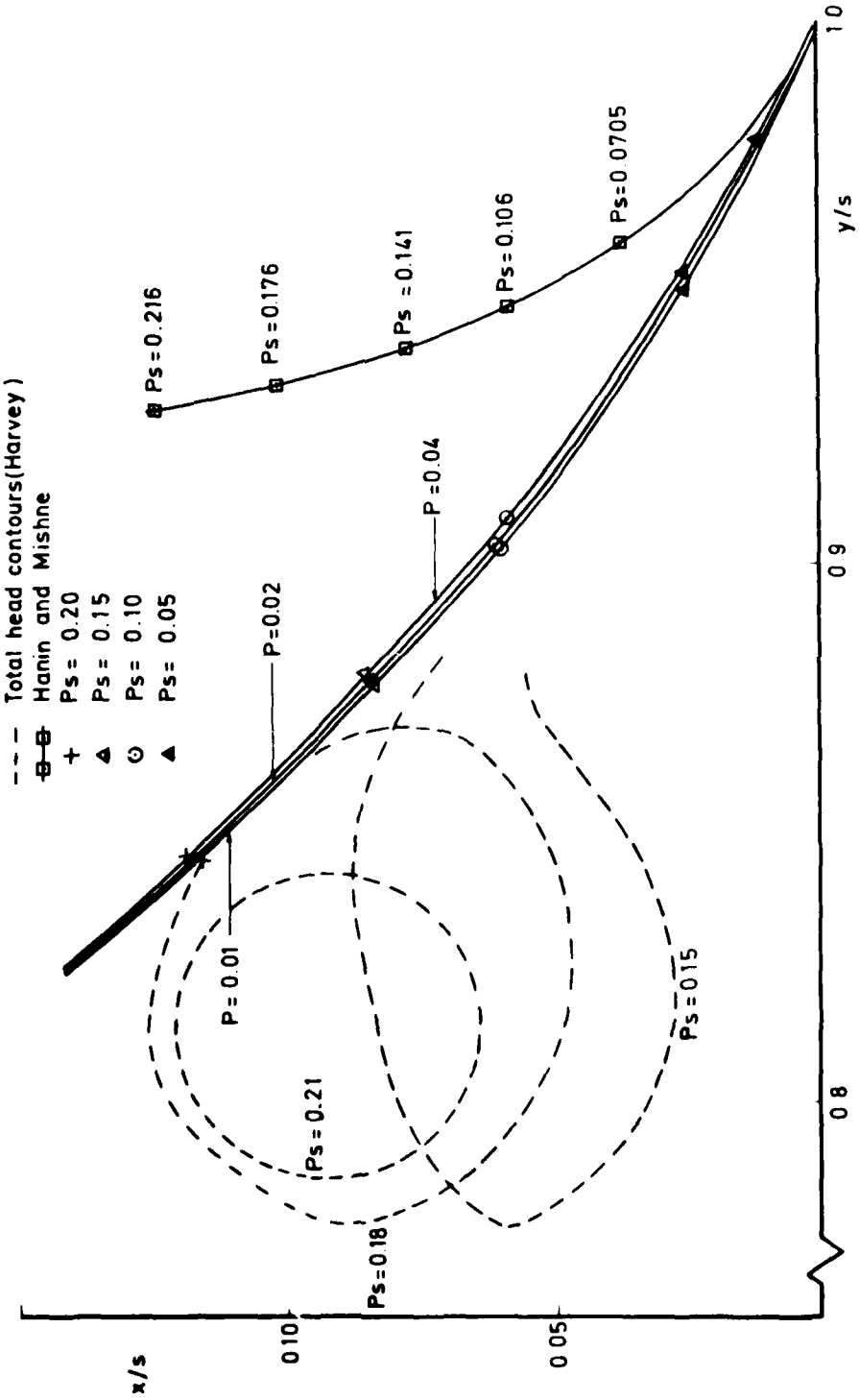

Fig 6 Vortex position

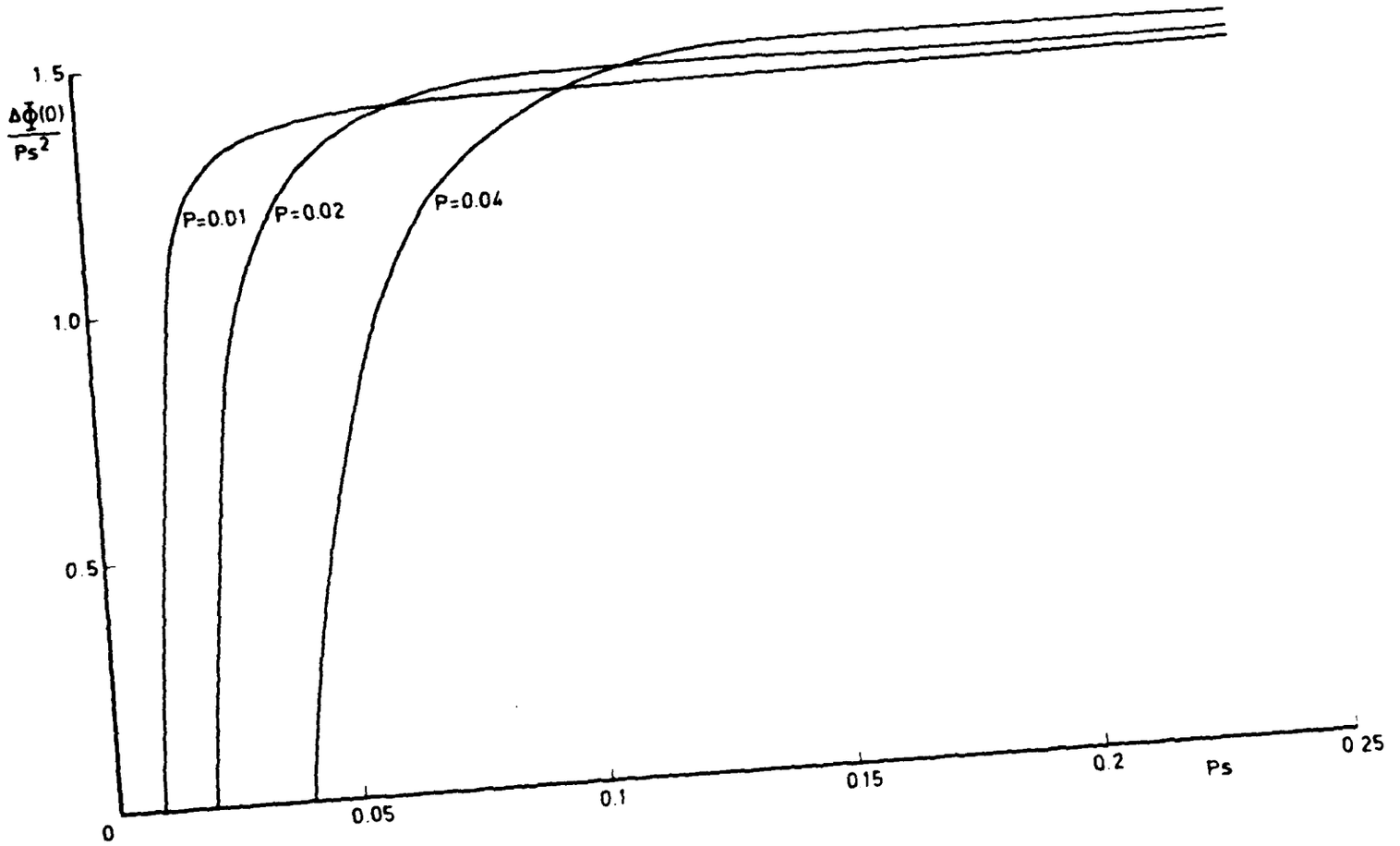

Fig 7 Total circulation

Fig 7

Fig 8

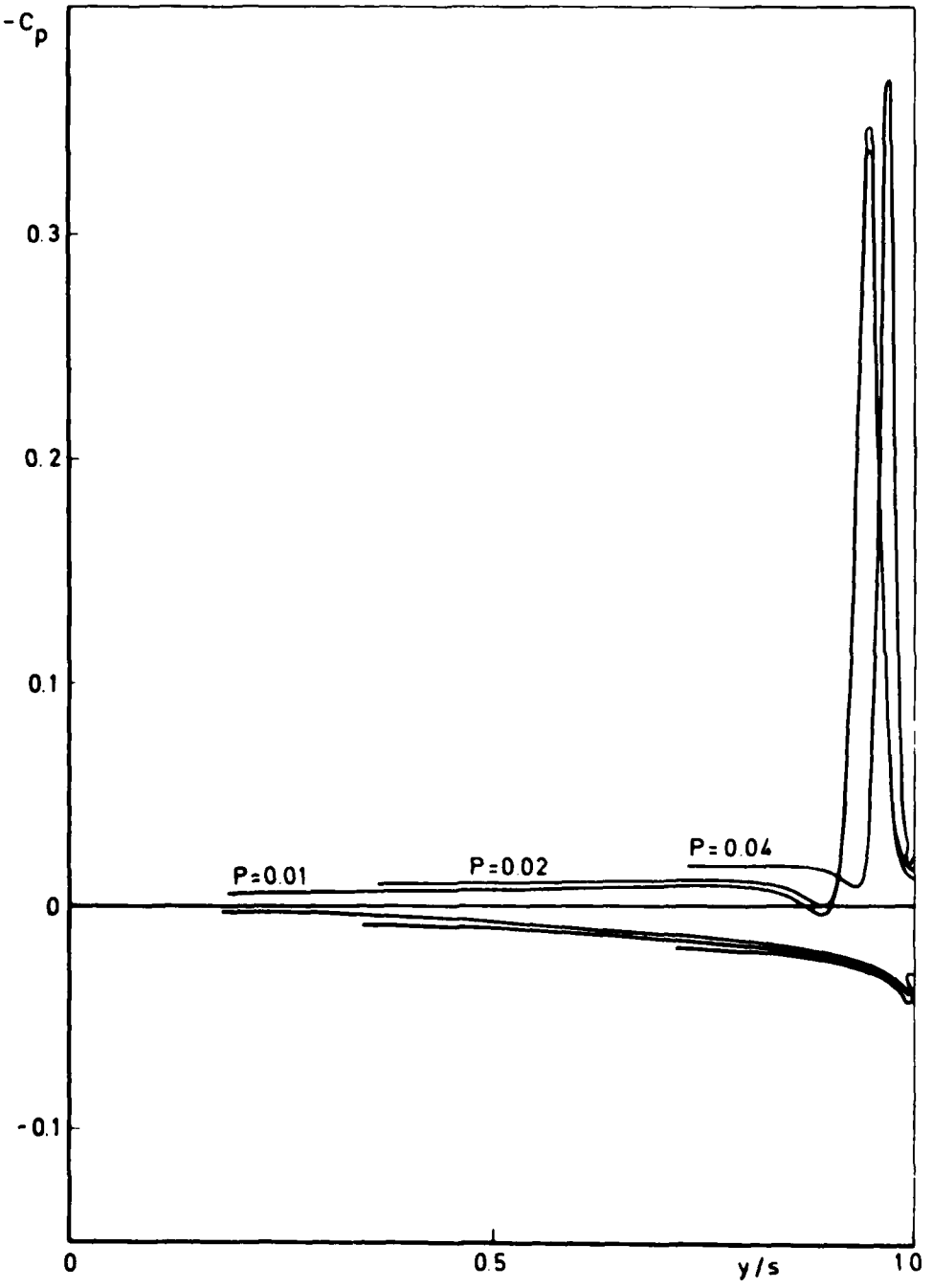

Fig 8 Pressure distribution on wing Ps = 0.0556

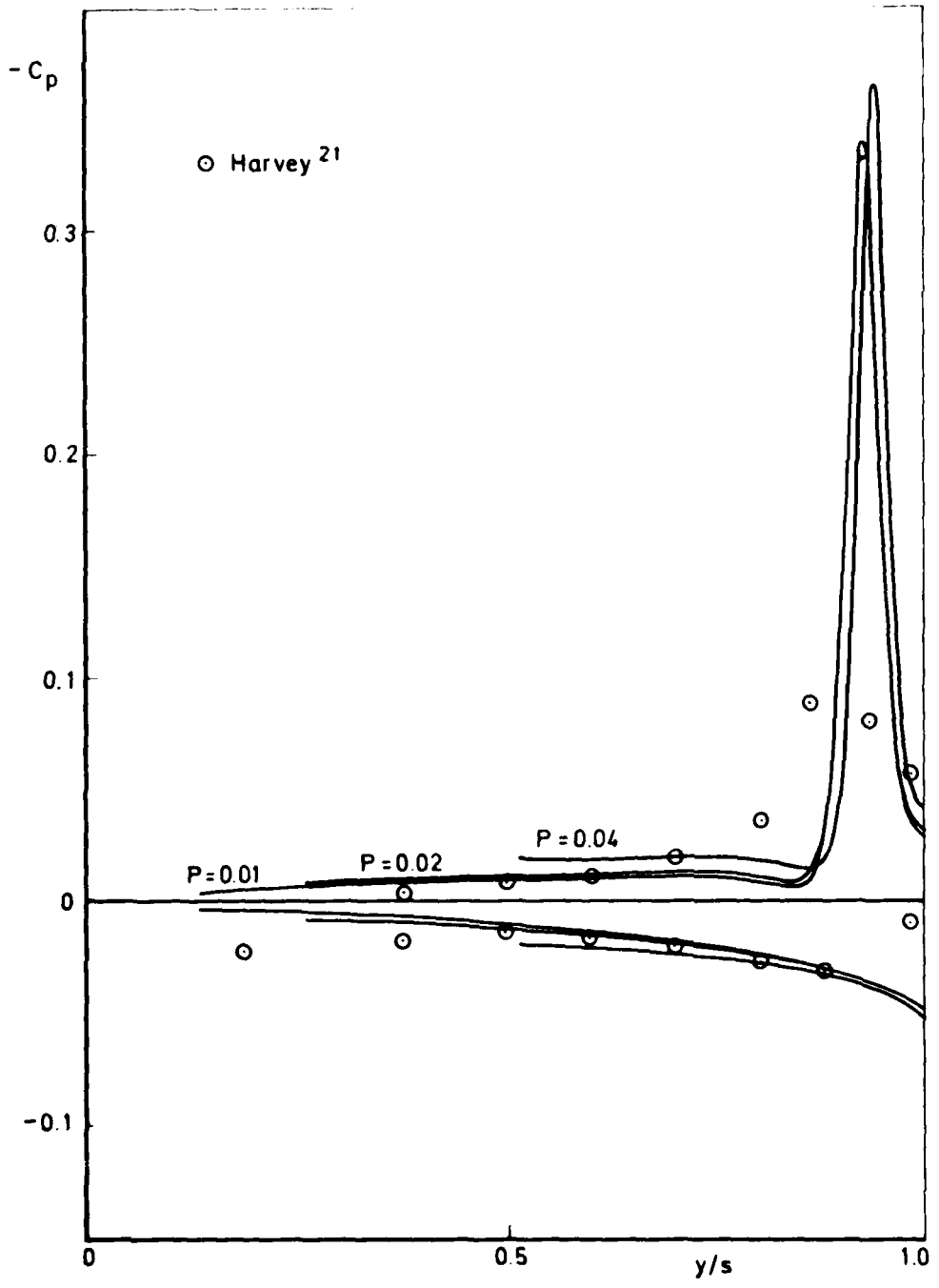

Fig 9 Pressure distribution on wing Ps = 0.0778

Fig 10

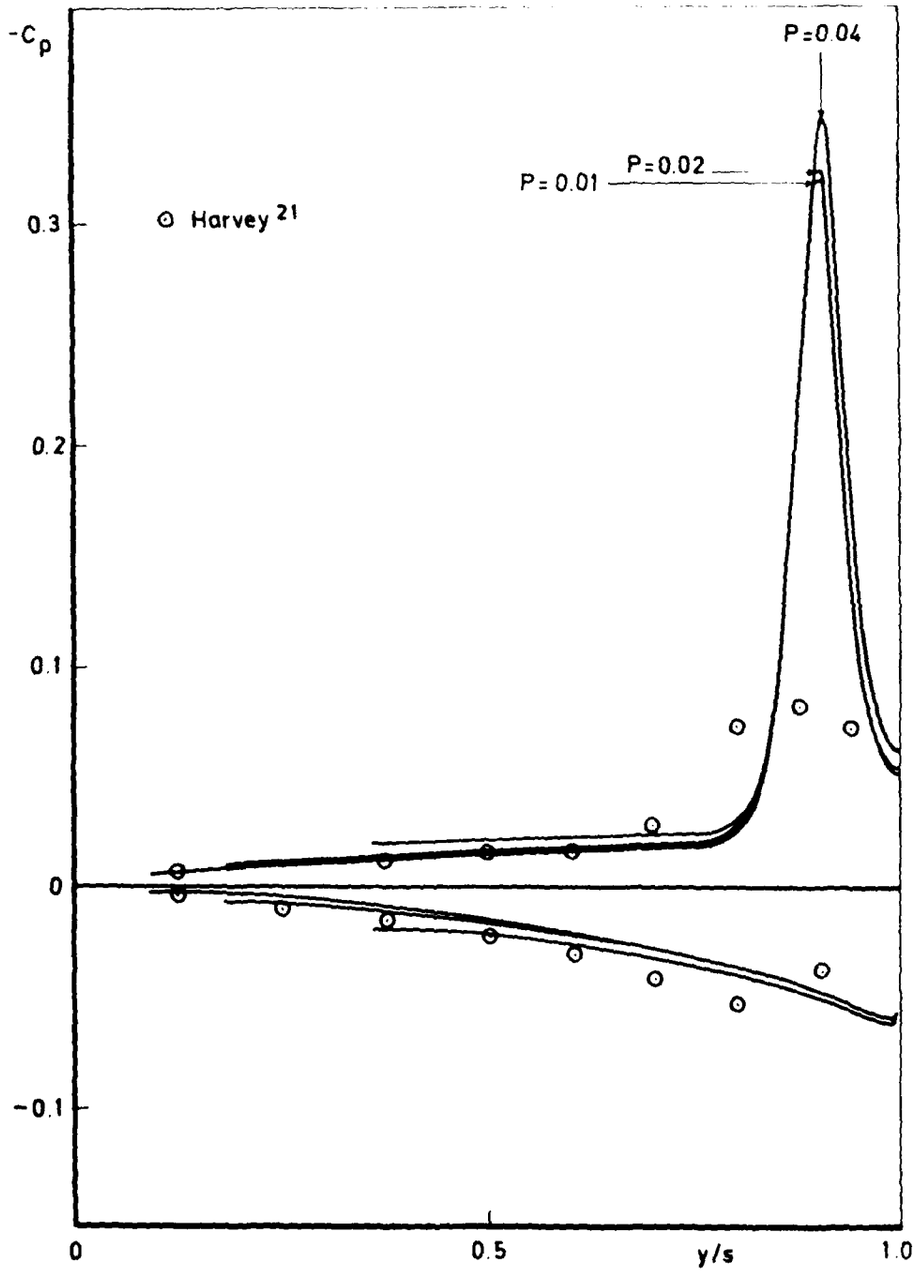

Fig 10 Pressure distribution on wing Ps = 0.1112

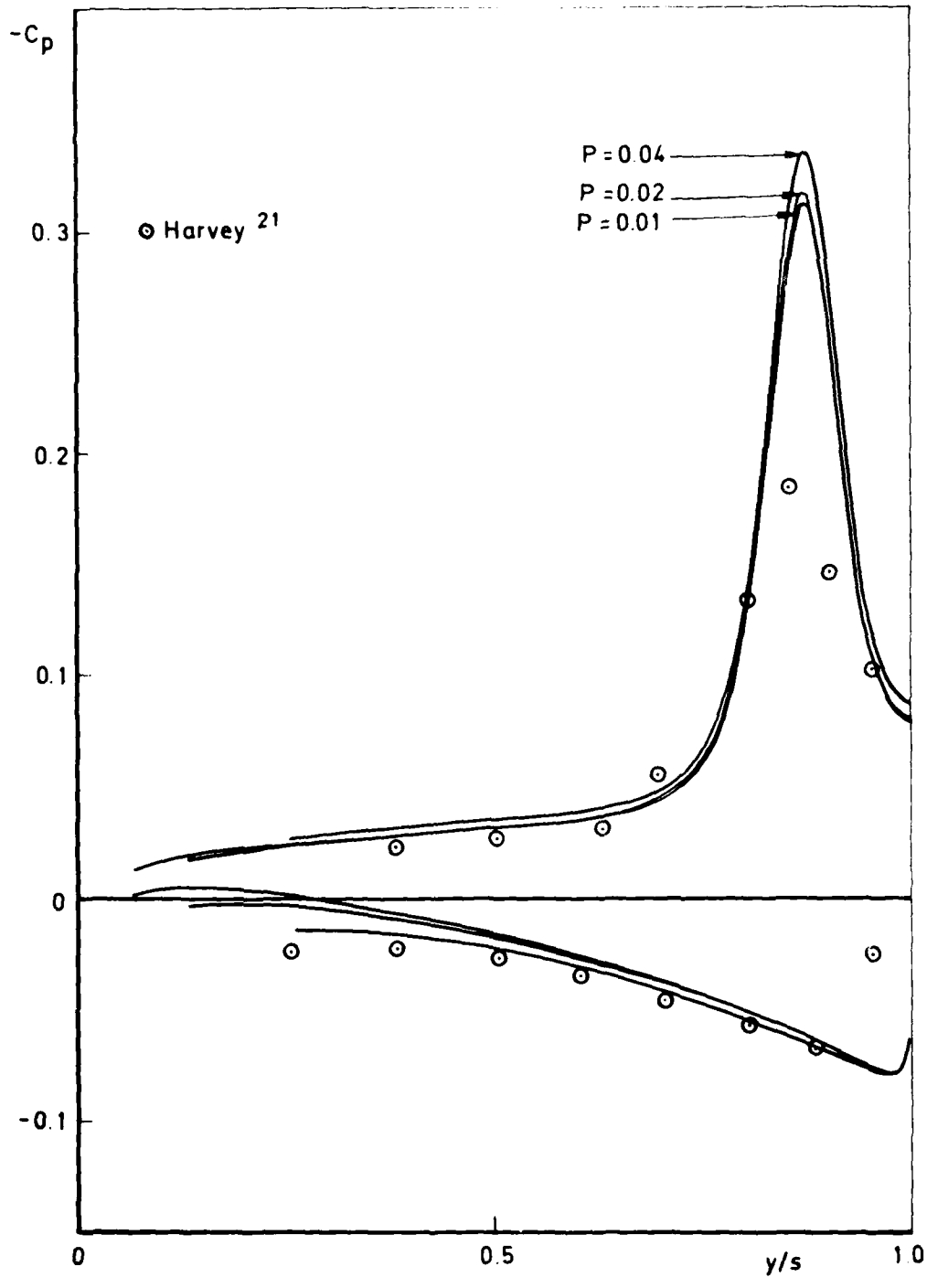

Fig 11 Pressure distribution on wing Ps = 0.1556

Fig 12

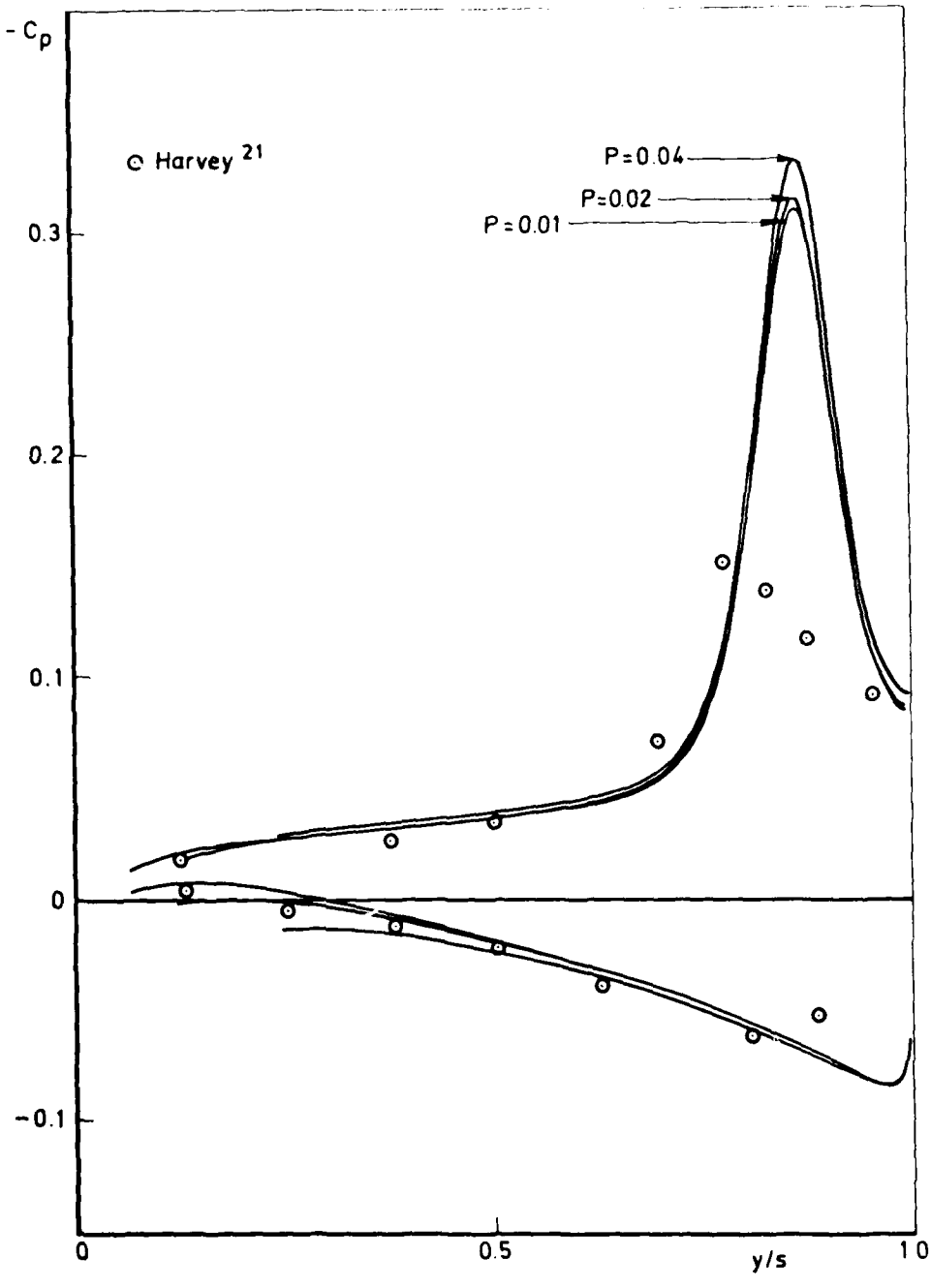

Fig 12 Pressure distribution on wing Ps = 0.1668

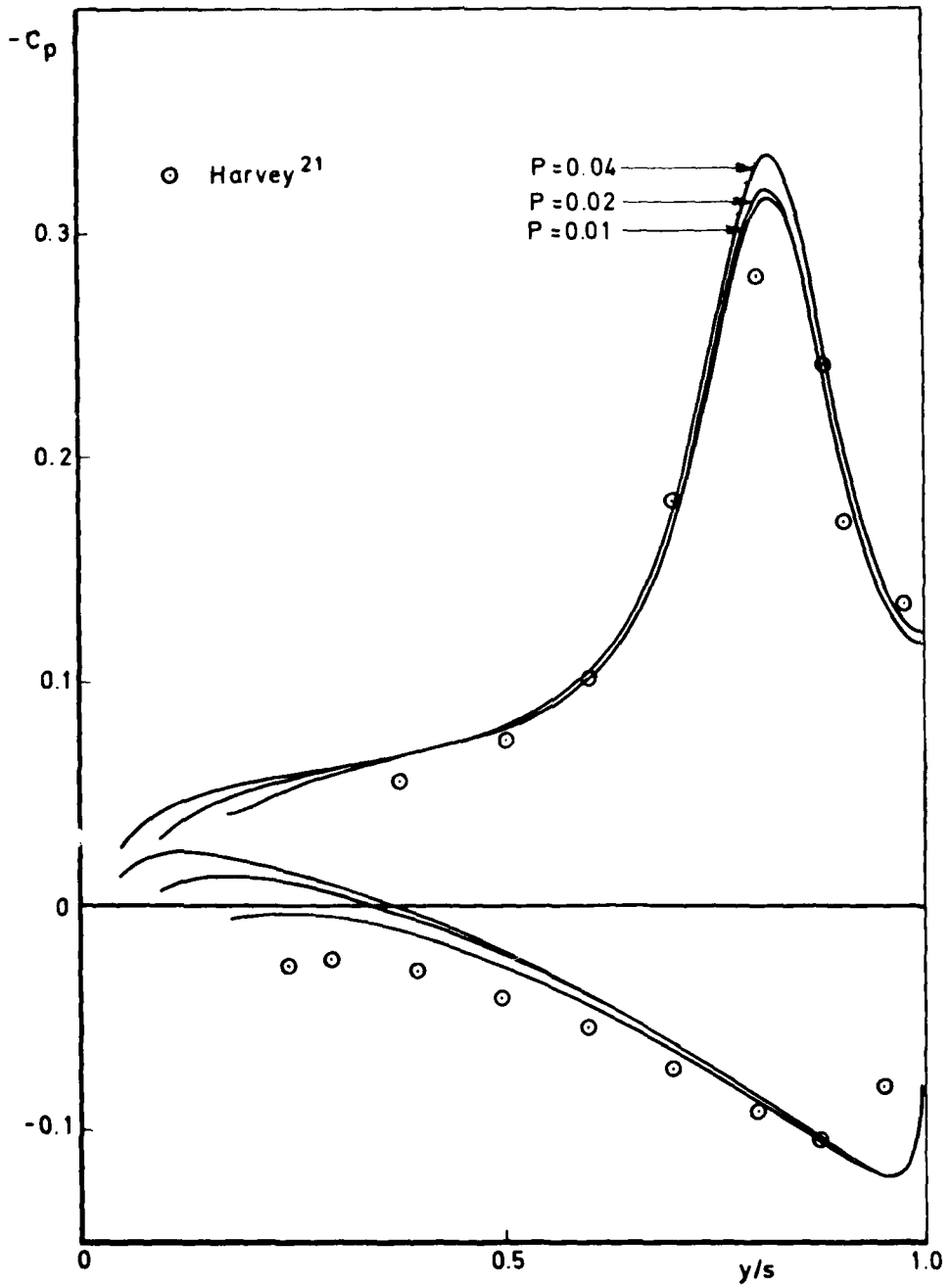

Fig 13 Pressure distribution on wing Ps = 0.2334

Fig 14

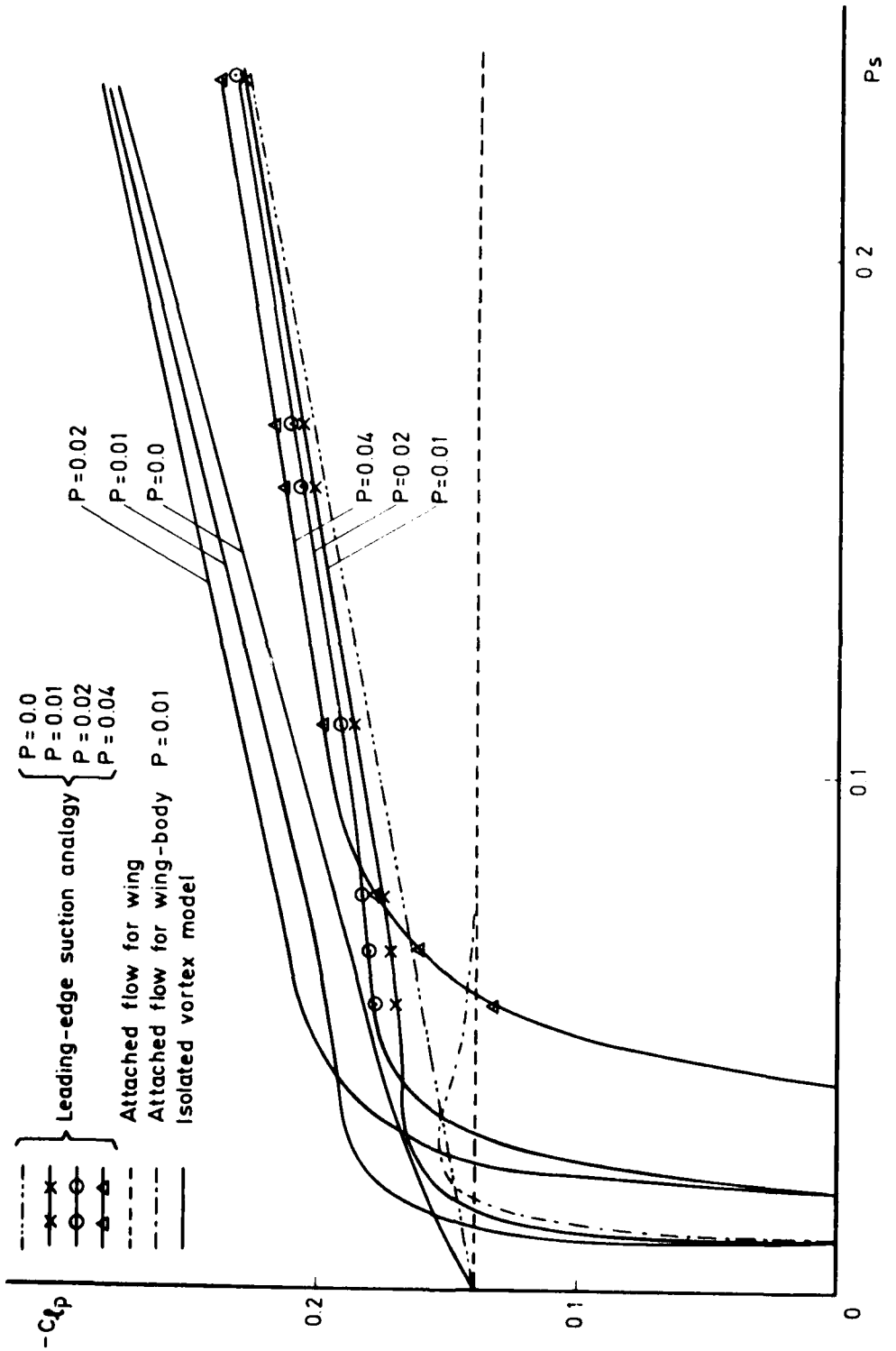

Fig 14 Local rolling moment coefficient; simple models

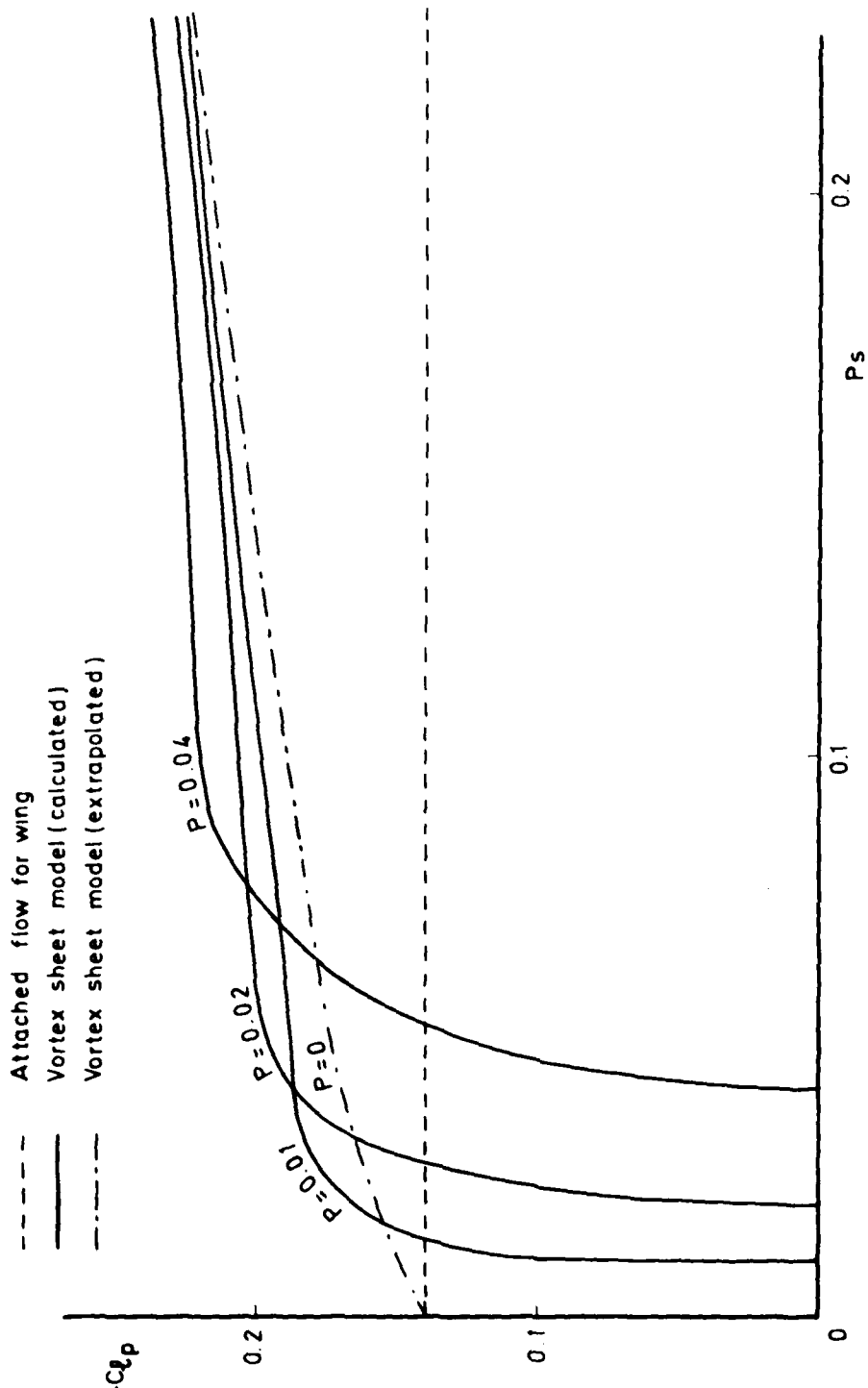

Fig 15 Local rolling moment coefficient; vortex sheet model

Fig 16

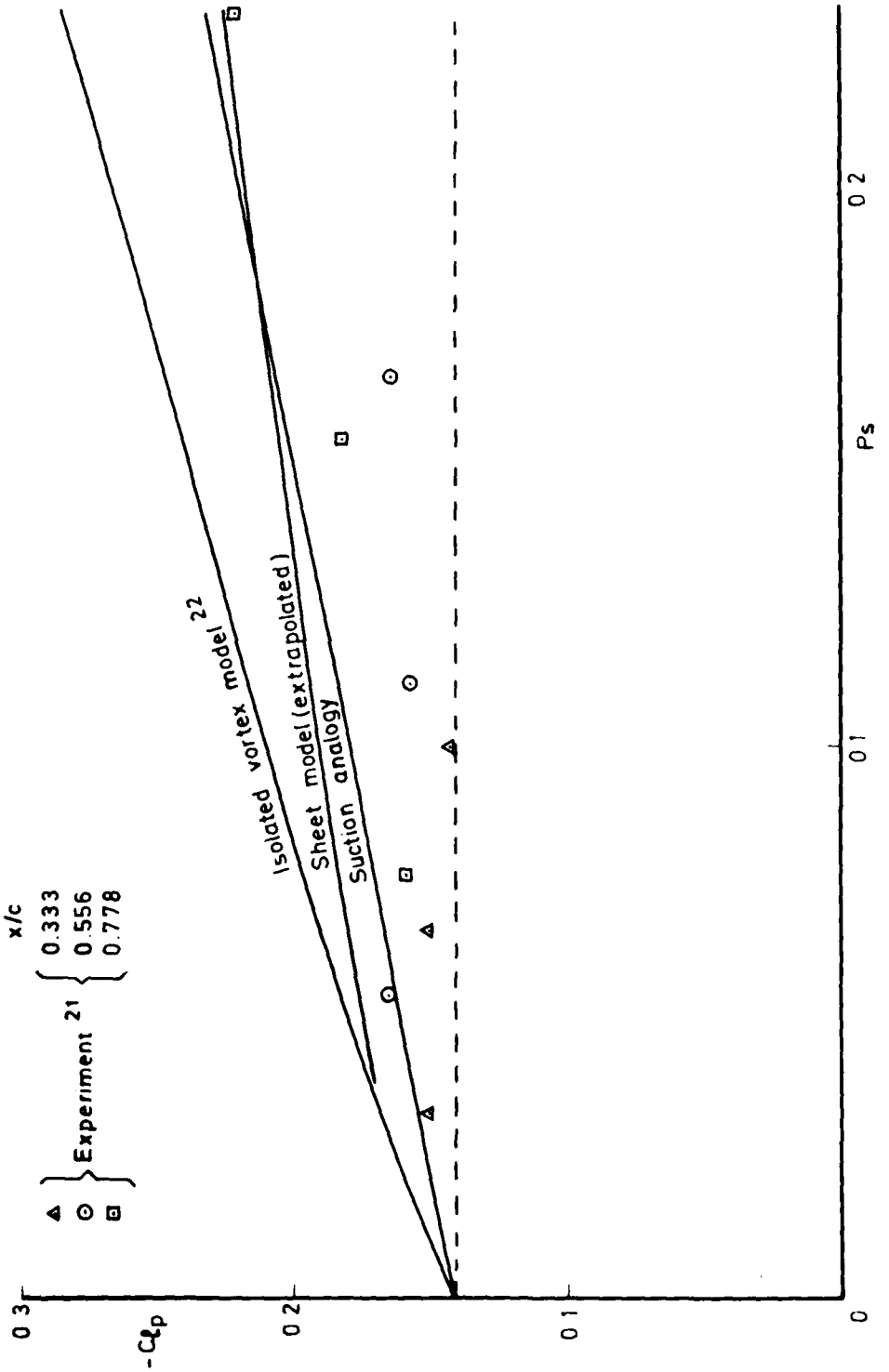

Fig 16 Local rolling moment coefficient; comparison of theory with experiment for delta wing

REPORT DOCUMENTATION PAGE

Overall security classification of this page

UNCLASSIFIED

As far as possible this page should contain only unclassified information. If it is necessary to enter classified information, the box above must be marked to indicate the classification, e.g. Restricted, Confidential or Secret.

1. DRIC Reference (to be added by DRIC)	2. Originator's Reference	3. Agency Reference	4. Report Security Classification/Marking
	RAE TR 80039	N/A	UNLIMITED

5. DRIC Code for Originator	6. Originator (Corporate Author) Name and Location
7673000W	Royal Aircraft Establishment, Farnborough, Hants, UK
5a. Sponsoring Agency's Code	6a. Sponsoring Agency (Contract Authority) Name and Location
N/A	N/A

7. Title Leading-edge separation from a slender rolling wing-body combination

7a. (For Translations) Title in Foreign Language

7b. (For Conference Papers) Title, Place and Date of Conference

8. Author 1. Surname, Initials	9a. Author 2	9b. Authors 3, 4	10. Date	Pages	Refs.
Jones, I.P.			March 1980	72	32

11. Contract Number	12. Period	13. Project	14. Other Reference Nos.
N/A	N/A		Aero 3476

15. Distribution statement
(a) Controlled by –
(b) Special limitations (if any) –

16. Descriptors (Keywords) (Descriptors marked * are selected from TEST)

Slender wing. Leading-edge vortex. Flow separation. Roll.

17. Abstract

A vortex-sheet model of the leading-edge separation is used to study the flow about a slender wing-body combination in steady rolling motion at zero incidence. The equations which model the flow are derived and the numerical method to solve these equations is described. The results presented concentrate on those values of the parameters for which comparison may be made with the experimental results of Harvey for a rolling delta wing. Results obtained using simplified flow models are also described.